Symplectic lattice gauge theories in the grid framework: Approaching the conformal window

Ed Bennett,[1,*] Peter A. Boyle,[2,3,†] Luigi Del Debbio,[4,‡] Niccolò Forzano,[5,§] Deog Ki Hong,[6,‖] Jong-Wan Lee,[6,7,8,¶] Julian Lenz,[1,**] C.-J. David Lin,[9,10,11,††] Biagio Lucini,[1,12,‡‡] Alessandro Lupo,[4,§§] Maurizio Piai,[5,‖‖] and Davide Vadacchino[13,¶¶]

[1]*Swansea Academy of Advanced Computing, Swansea University (Bay Campus), Fabian Way, SA1 8EN Swansea, Wales, United Kingdom*
[2]*School of Physics and Astronomy, University of Edinburgh, Edinburgh EH9 3FD, United Kingdom*
[3]*Physics Department, Brookhaven National Laboratory, Upton, New York 11973, USA*
[4]*Higgs Centre for Theoretical Physics, School of Physics and Astronomy, The University of Edinburgh, Peter Guthrie Tait Road, Edinburgh EH9 3FD, United Kingdom*
[5]*Department of Physics, Faculty of Science and Engineering, Swansea University, Singleton Park, SA2 8PP, Swansea, Wales, United Kingdom*
[6]*Department of Physics, Pusan National University, Busan 46241, Korea*
[7]*Institute for Extreme Physics, Pusan National University, Busan 46241, Korea*
[8]*Particle Theory and Cosmology Group, Center for Theoretical Physics of the Universe, Institute for Basic Science (IBS), Daejeon, 34126, Korea*
[9]*Institute of Physics, National Yang Ming Chiao Tung University, 1001 Ta-Hsueh Road, Hsinchu 30010, Taiwan*
[10]*Centre for High Energy Physics, Chung-Yuan Christian University, Chung-Li 32023, Taiwan*
[11]*Centre for Theoretical and Computational Physics, National Yang Ming Chiao Tung University, 1001 Ta-Hsueh Road, Hsinchu 30010, Taiwan*
[12]*Department of Mathematics, Faculty of Science and Engineering, Swansea University (Bay Campus), Fabian Way, SA1 8EN Swansea, Wales, United Kingdom*
[13]*Centre for Mathematical Sciences, University of Plymouth, Plymouth, PL4 8AA, United Kingdom*

(Received 19 July 2023; accepted 24 October 2023; published 20 November 2023)

Symplectic gauge theories coupled to matter fields lead to symmetry enhancement phenomena that have potential applications in such diverse contexts as composite Higgs, top partial compositeness, strongly interacting dark matter, and dilaton-Higgs models. These theories are also interesting on theoretical grounds, for example in reference to the approach to the large-N limit. A particularly compelling research aim is the determination of the extent of the conformal window in gauge theories with symplectic groups coupled to matter, for different groups and for field content consisting of fermions transforming in different representations. Such determination would have far-reaching implications, but requires overcoming huge technical challenges. Numerical studies based on lattice field theory can provide the quantitative information necessary to this endeavor. We developed new software to implement symplectic groups in the Monte Carlo algorithms within the Grid framework. In this paper, we focus most of our attention on the $Sp(4)$ lattice gauge theory coupled to four (Wilson-Dirac) fermions transforming in the 2-index

*E.J.Bennett@swansea.ac.uk
†pboyle@bnl.gov
‡luigi.del.debbio@ed.ac.uk
§2227764@swansea.ac.uk
‖dkhong@pusan.ac.kr
¶j.w.lee@ibs.re.kr
**j.j.lenz@swansea.ac.uk
††dlin@nycu.edu.tw
‡‡B.Lucini@Swansea.ac.uk
§§Alessandro.Lupo@ed.ac.uk
‖‖m.piai@swansea.ac.uk
¶¶davide.vadacchino@plymouth.ac.uk

antisymmetric representation, as a case study. We discuss an extensive catalog of technical tests of the algorithms and present preliminary measurements to set the stage for future large-scale numerical investigations. We also include the scan of parameter space of all asymptotically free $Sp(4)$ lattice gauge theories coupled to varying number of fermions transforming in the antisymmetric representation.

DOI: 10.1103/PhysRevD.108.094508

I. INTRODUCTION

Gauge theories with symplectic group, $Sp(2N)$, in four space-time dimensions have been proposed as the microscopic origin of several new physics models that stand out in the literature for their simplicity and elegance. We list some compelling examples later in this introduction. Accordingly, lattice field theory methods have been deployed to obtain numerically a first quantitative characterization of the strongly coupled dynamics of such gauge theories [1–19]. Different regions of lattice parameter space have been explored; by varying the rank of the group, N, the number, $N_{\mathrm{f,\,as}}$, and mass, $m^{\mathrm{f,as}}$, of (Dirac) fermions transforming in the fundamental (f) and 2-index antisymmetric (as) representation, one can tabulate the properties of these theories. And, after taking infinite volume and continuum limits, the results can be used by model builders, phenomenologists, and field theorists working on potential applications.

A prominent role in the recent literature is played by the theory with $N = 2$, $N_{\mathrm{f}} = 2$, and $N_{\mathrm{as}} = 3$. It gives rise, at low energies, to the effective field theory (EFT) entering the minimal Composite Higgs model (CHM) that is amenable to lattice studies [20],[1] and also realizes top (partial) compositeness [85] (see also Refs. [86,87]). It hence provides an economical way of explaining the microscopic origin of the two heaviest particles in the standard model, the Higgs boson and the top quark, singling them out as portals to new physics.

The $Sp(2N)$ gauge theories with $N_{\mathrm{f}} = 2$ and $N_{\mathrm{as}} = 0$ find application also in the simplest realizations of the strongly interacting massive particle (SIMP) scenario for dark matter [88–96]. They can address observational puzzles such as the *core vs. cusp* [97] and *too big to fail* [98] problems. In addition, they might have profound implications in the physics of the early universe and be testable in present and future gravitational wave experiments [99–116]. This is because they can give rise to a relic stochastic background of gravitational waves [117–122], that are the current subject of active study [123–125].

On a more abstract, theoretical side, in $Sp(2N)$ Yang-Mills theories one can compute numerically the spectra of glueballs and strings [126–135], as well as the topological charge and susceptibility [136–152]. This allows for a comparison with other gauge groups ($SU(N_c)$ in particular), by means of which to test nonperturbative ideas about field theories and their approach to the large-N_c limit—see, e.g., Refs. [5,10,153–155]. Indeed, even the pioneering lattice study of symplectic theories in Ref. [156] was performed to the purpose of better characterizing on general grounds the deconfinement phase transition.

A special open problem is that of the highly nontrivial determination of the extent of the conformal window in strongly coupled gauge theories with matter field content. It has both theoretical and phenomenological implications, of general interest to model-builders, phenomenologists, and field theorists alike. Particular attention has been so far paid to $SU(N_c)$ theories, more than $Sp(2N)$ (with $N > 1$) ones. Let us pause and explain what the problem is, on general grounds. Robust perturbation-theory arguments show that if the number of matter fields is large enough—but not so much as to spoil asymptotic freedom—gauge theories can be realized in a conformal phase. This is the case when long distance physics is governed by a fixed point of the renormalization group (RG) evolution [157,158], and the fixed point is described by a conformal field theory (CFT). It is reasonable to believe that such fixed points may exist also outside the regime of validity of perturbation theory, when the number of matter fields is smaller. What is the smallest number of fermions for which the theory still admits a fixed point, rather than confining in the infrared (IR), is an open question. While gaining some control over nonperturbative physics is possible in supersymmetric theories (see Ref. [159] and references therein), the non-supersymmetric ones are the subject of a rich and fascinating literature [160–168], part of which uses perturbative instruments and high-loop expansions [169–181], but there is no firm agreement on the results—we include a brief overview of work in this direction, in the body of the paper.

Knowledge of the extent of the conformal window also has relevant phenomenological implications. Various arguments suggest that at the lower edge of the conformal window, the anomalous dimensions of the CFT operators might be so large as to invalidate naive dimensional analysis (NDA) expectations for the scaling of observable quantities [161,182]. And it has been speculated that this might affect even confining theories that live outside the

[1]The literature on CHMs in which the Higgs fields emerge as pseudo-Nambu-Goldstone bosons (PNGBs) from the spontaneous breaking of the approximate global symmetries of a new, strongly coupled theory [21–23], is vast. See, e.g., the reviews in Refs. [24–26], the summary tables in Refs. [27–29], and the selection of papers in Refs. [30–84].

conformal window, with applications to technicolor, CHMs, top (partial) compositeness, SIMP dark matter (e.g., see Refs. [24–26,183–188] and references therein).

Lattice studies of the extent of the conformal window have mostly focused on $SU(N_c)$ groups, with fermion matter in various representations of the gauge group.[2] Closely related to these studies is the emergence, in $SU(3)$ gauge theories with eight (Dirac) fermions transforming in the fundamental representation [242–250], or (Dirac) fermions transforming in the 2-index symmetric representation [251–256], of numerical evidence pointing to the existence of a light isosinglet scalar state, that is tempting to identify with the dilaton, the PNGB associated with dilatations.

It has been predicted long ago that a light dilaton should exist in strongly coupled, confining theories living in proximity of the lower end of the conformal window [257–259], and the EFT description of such state has a remote historical origin [260,261]. It might have huge consequences in extensions of the standard model [262]. A plethora of phenomenological studies exists on the dilaton (see, for example, Refs. [263–274] and references therein). The $SU(3)$ lattice evidence for the existence of this state has triggered renewed interest in the dilaton effective field theory (dEFT), which combines the chiral Lagrangian description of the PNGBs associated with the internal global symmetries of the system, with the additional, light scalar, interpreted as a dilaton [275–290].

The aforementioned lattice studies of symplectic theories, motivated by CHMs and SIMPs, can be carried out with comparatively modest resources, and using lattices of modest sizes, because they require exploring the intermediate mass range for the mesons in the theory. By contrast, the study of the deep-IR properties of $Sp(2N)$ gauge theories requires investigating the low mass regime of the fermions, for which one needs lattices and ensembles big enough to overcome potentially large finite size effects and long autocorrelation times. The supercomputing demands (both on hardware and software) of these calculations are such that a new dedicated set of instruments, and a long-term research strategy, is needed to make these investigations feasible. With this paper, we make the first, propaedeutic, technical steps on the path toward determining on the lattice the extent of the conformal window in theories with $Sp(2N)$ group, for $N > 1$.

To this end, we elected to build, test, and make publicly available new software [291], that supplements previous releases of the Grid library [292–295], by adding to it new functionality specifically designed to handle $Sp(2N)$ theories with matter fields in multiple representations. The resulting software takes advantage of all the features offered by the modularity and flexibility of Grid, in particular its ability to work both on CPU- as well as GPU-based architectures. We present two types of preliminary results relevant to this broader endeavor: technical tests of the algorithm and of the physics outcomes are supplemented by preliminary analyses, conducted on coarse lattices, of the parameter space of the lattice theory. The latter set the stage for future large-scale numerical studies, by identifying the regions of parameter space connected to continuum physics. The former are intended to validate the software, and test its performance for symplectic theories on machines with GPU architecture. Unless otherwise specified, we use the $Sp(4)$ theory, coupled to $N_{\rm as} = 4$ Wilson-Dirac fermions transforming in the 2-index antisymmetric representation, as a case study. The lessons we learn from the results we report have general validity and applicability.

This paper is organized as follows. We start by defining the $Sp(2N)$ gauge theories of interest in Sec. II, both in the continuum and on the lattice. We also summarize briefly the current understanding of the extent of the conformal window in these theories. Section III discusses the software implementation of $Sp(2N)$ on Grid, and the basic tests we performed on the algorithm. In Sec. IV we concentrate on lattice theories in which the fermions do not contribute to the dynamics, focusing both on the Yang-Mills theory and the quenched approximation. New results about the bulk structure of all the $Sp(4)$ theories coupled to (Wilson-Dirac) fermions transforming in the 2-index antisymmetric representation can be found in Sec. V, while Sec. VI discusses scale setting (Wilson flow) and topology. A brief summary and outlook concludes the paper, in Sec. VII. Additional technical details are relegated to the appendix.

II. GAUGE THEORIES WITH SYMPLECTIC GROUP

The $Sp(2N)$ continuum field theories of interest (with $N > 1$), written in Minkowski space with signature mostly '−', have the following Lagrangian density (we borrow notation and conventions from Ref. [4]):

$$\begin{aligned}\mathcal{L} = &-\frac{1}{2}\mathrm{Tr} G_{\mu\nu}G^{\mu\nu} + \frac{1}{2}\sum_{i}^{N_{\rm f}} (i\overline{Q^i}_a \gamma^\mu (D_\mu Q^i)^a - i\overline{D_\mu Q^i}_a \gamma^\mu Q^{ia}) \\ &- m^{\rm f}\sum_{i}^{N_{\rm f}} \overline{Q^i}_a Q^{ia} \\ &+ \frac{1}{2}\sum_{k}^{N_{\rm as}} (i\overline{\Psi^k}_{ab} \gamma^\mu (D_\mu \Psi^k)^{ab} - i\overline{D_\mu \Psi^k}_{ab} \gamma^\mu \Psi^{kab}) \\ &- m^{\rm as}\sum_{k}^{N_{\rm as}} \overline{\Psi^k}_{ab} \Psi^{kab}. \end{aligned} \tag{1}$$

The fields Q^{ia}, with $i = 1, \ldots, N_{\rm f}$, are Dirac fermions that transform in the fundamental representation of $Sp(2N)$, as

[2] See for instance the review in Ref. [189], and references therein, in particular Refs. [190–241].

indicated by the index $a = 1, \ldots, 2N$, while the Ψ^{kab} ones, with $k = 1, \ldots, N_{\rm as}$, transform in the 2-index antisymmetric representation of the gauge group. The covariant derivatives are defined by making use of the transformation properties under the action of an element U of the $Sp(2N)$ gauge group, according to which

$$Q \to UQ, \quad \text{and} \quad \Psi \to U\Psi U^{\rm T}. \tag{2}$$

They can be written in terms of the gauge field $A_\mu \equiv A_\mu^a t^a$, where t^a are the generators of $Sp(2N)$, normalized so that $\mathrm{Tr}\ t^a t^b = \frac{1}{2}\delta^{ab}$, to read as follows:

$$D_\mu Q^i = \partial_\mu Q^i + igA_\mu Q^i, \tag{3}$$

$$D_\mu \Psi^j = \partial_\mu \Psi^j + igA_\mu \Psi^j + ig\Psi^j A_\mu^{\rm T}, \tag{4}$$

where g is the gauge coupling. The field-strength tensor is given by

$$G_{\mu\nu} \equiv \partial_\mu A_\nu - \partial_\nu A_\mu + ig[A_\mu, A_\nu], \tag{5}$$

where $[\cdot,\cdot]$ is the commutator.

The form of Eq. (1) makes it easy to show that the $SU(N_{\rm f})_L \times SU(N_{\rm f})_R$ and $SU(N_{\rm as})_L \times SU(N_{\rm as})_R$ global symmetries acting on the flavor indexes of Q^i and Ψ^k, respectively, are enhanced to $SU(2N_{\rm f})$ and $SU(2N_{\rm as})$. By rewriting Eq. (1) in terms of 2-component fermions [4,296], see Refs. [4,296] for details.

$$Q^{ia} = \begin{pmatrix} q^{ia} \\ \Omega^{ab}(-\tilde{C}q^{i+2,*})_b \end{pmatrix},$$
$$\Psi^{kab} = \begin{pmatrix} \psi^{kab} \\ \Omega^{ab}\Omega^{bd}(-\tilde{C}q^{k+3,*})_{cd} \end{pmatrix}, \tag{6}$$

($\tilde{C} = -i\tau^2$, τ^2 is the second Pauli matrix) we get the Lagrangian where the global symmetries are manifest

$$\mathcal{L} = -\frac{1}{2}\mathrm{Tr}G_{\mu\nu}G^{\mu\nu} + \frac{1}{2}\sum_j^{2N_{\rm f}}(i(q^j)_a^\dagger \bar{\sigma}^\mu (D_\mu q^j)^a - i(D_\mu q^j)_a^\dagger \bar{\sigma}^\mu (q^j)^a) - \frac{1}{2}m^{\rm f}\sum_{j,k}^{2N_{\rm f}}\Omega_{jk}(q^{jaT}\Omega_{ab}\tilde{C}q^{kb} - (q^j)_a^\dagger \Omega^{ab}\tilde{C}(q^{k*})_b)$$
$$+\frac{1}{2}\sum_k^{2N_{\rm as}}(i(\psi^k)_{ab}^\dagger \bar{\sigma}^\mu (D_\mu \psi^k)^{ab} - i(D_\mu \psi^k)_{ab}^\dagger \bar{\sigma}^\mu (\psi^k)^{ab}) - \frac{1}{2}m^{\rm as}\sum_{j,k}^{2N_{\rm as}}\omega_{jk}(\psi^{jabT}\Omega_{ac}\Omega_{bd}\tilde{C}\psi^{kcd} - (\psi^j)_{ab}^\dagger \Omega^{ac}\Omega^{bd}\tilde{C}(\psi^{k*})_{cd}), \tag{7}$$

where we defined $\bar{\sigma}^\mu \equiv (\mathbb{1}_{2\times 2}, \tau^i)$ and $\omega_{jk} = \omega^{jk} \equiv \left(\begin{smallmatrix} 0 & \mathbb{1}_{N_{\rm as}} \\ \mathbb{1}_{N_{\rm as}} & 0 \end{smallmatrix}\right)$. The antisymmetric matrix Ω has the same form, as defined in Eq. (A1) of Appendix A, for both the gauge and fundamental flavor symmetries, but the indices run with $a = 1, \ldots, 2N$ for the former and with $j = 1, \ldots, 2N_{\rm f}$ for the latter.

The mass terms break the symmetries to the maximal $Sp(2N_{\rm f})$ and $SO(2N_{\rm as})$ subgroups. Bilinear fermion condensates arise nonperturbatively, breaking the symmetries according to the same pattern, and hence one expects the presence of $N_{\rm f}(2N_{\rm f}-1)-1$ PNGBs in the (f) sector (for $N_f > 1$), and $N_{\rm as}(2N_{\rm as}+1)-1$ in the (as) sector.

The main parameters governing the system are hence N, $N_{\rm f}$, and $N_{\rm as}$, and in most of the paper we refer to the theory with $N = 2$, $N_{\rm f} = 0$, and $N_{\rm as} = 4$ as a case study. The running coupling, g, obeys a renormalization group equation (RGE) in which the beta function at the 1-loop order is scheme-independent,

$$\beta = -\frac{g^3}{(4\pi)^2}b_1, \tag{8}$$

and is governed by the coefficient b_1, which for a non-Abelian theory coupled to Dirac fermions can be written as

$$b_1 = \frac{11}{3}C_2(G) - \frac{4}{3}N_{\rm f}\frac{d_{\rm f}}{d_G}C_2({\rm f}) - \frac{4}{3}N_{\rm as}\frac{d_{\rm as}}{d_G}C_2 \quad ({\rm as}) \tag{9}$$

and, specifically for $Sp(2N)$ groups, becomes

$$b_1 = \frac{11}{3}(N+1) - \frac{2}{3}N_{\rm f} - \frac{4}{3}N_{\rm as}\frac{N(2N-1)-1}{N(2N+1)}N. \tag{10}$$

The coefficients $C_2(G)$, $C_2({\rm f})$, $C_2({\rm as})$ are quadratic Casimir operators in the adjoint, fundamental and antisymmetric representations, while d_G, $d_{\rm f}$, $d_{\rm as}$ are the dimensions of these representations, respectively. We restrict attention to asymptotically free theories, for which b_1 is positive. For $Sp(2N)$ theories with $N_{\rm f} = 0$, this requirement sets the upper bound $N_{\rm as} < \frac{11(N+1)}{4(N-1)}$, which for $N = 2$ yields $N_{\rm as} < 33/4$—perturbatively, as-type fermions make double the contribution of f-type ones, in $Sp(4)$. The spectrum of mesons depends on the mass, $m^{\rm f,as}$, of the fermions, by varying which we can test which of the following three possible classes the theory falls into.

(i) The theory confines, similarly to Yang-Mills theories. One expects to find a gapped spectrum, and a set of PNGBs that become parametrically light in respect to other states, when $m^{\rm f,as} \to 0$. The small

mass and momentum regime is described by chiral perturbation theory (χPT) [297–300].

(ii) The theory is IR conformal. In this case, a gap arises only because of the presence of the mass terms, and would disappear into a continuum for $m^{\mathrm{f,as}} \to 0$. The spectrum and spectral density exhibit scaling, in the form described for example in Refs. [195,301–306]—see also Ref. [307].

(iii) The theory is confining, but has near-conformal dynamics. As in the confining case, when $m^{\mathrm{f,as}} \to 0$ one finds massless PNGBs. An additional isosinglet scalar state, the dilaton, is also light, compared to the other mesons, and long distance physics is described by dEFT [275–290]—see also the discussions in Refs. [308–310], and references therein.

A. The conformal window

The three possible classes of gauge theories described above are determined by whether the theory is, respectively, far outside, inside or just outside the boundary of the conformal window. The determination of the conformal window is tantamount to showing the existence of the IR fixed point at nonzero coupling so that the theory is interacting and IR conformal. We provide here some more detail and information about this challenging endeavor and what is known to date, starting from perturbative arguments. The coefficient of the (scheme-independent) 2-loop RG beta function, b_2, which is found to be, for generic non-Abelian gauge theories,

$$b_2 = \frac{34}{3} C_2(G)^2 - \frac{4}{3}(5C_2(G) + 3C_2(\mathrm{f}))\frac{d_{\mathrm{f}}}{d_G} C_2(\mathrm{f}) N_{\mathrm{f}} - \frac{4}{3}(5C_2(G) + 3C_2(\mathrm{as}))\frac{d_{\mathrm{as}}}{d_G} C_2(\mathrm{as}) N_{\mathrm{as}}, \tag{11}$$

and for $Sp(2N)$ groups reduces to

$$b_2 = \frac{34}{3}(N+1)^2 - \frac{2}{3} N_{\mathrm{f}} \left[5(N+1) + \frac{3}{4}(2N+1)\right] - \frac{4}{3} N_{\mathrm{as}} [3N + 5(N+1)] \frac{N(2N-1)-1}{2N+1}, \tag{12}$$

When b_2 is negative, one finds that for a positive and sufficiently small value of b_1, a perturbative IR fixed point at coupling $\alpha_{\mathrm{IR}} \simeq \alpha_{\mathrm{BZ}} = -4\pi b_1/b_2 \ll 1$ arises. This is referred to as a Banks-Zaks (BZ) fixed point [157,158]. The upper bound of the conformal window therefore coincides with that of asymptotically free theories, given by $b_1 = 0$.

The determination of the lower bound of the conformal window is hindered by the vicinity of the strong coupling regime. To see this, one can fix the value of N and decrease the number of flavors $N_{\mathrm{f,as}}$. The coefficient b_2 then becomes less negative and eventually approaches zero, while b_1 remains finite and positive. Accordingly, the coupling at the (perturbative) BZ fixed point, α_{BZ}, becomes larger and larger and the perturbative analysis of the β function is no longer reliable. Despite such inherent limitations, several (approximate) analytical methods have been proposed to estimate the critical value $N^{\mathrm{cr}}_{\mathrm{f,as}}$ corresponding to the lower edge of the conformal window. We now briefly summarize known results, for the theories of interests, that can be used to guide dedicated studies using nonperturbative numerical techniques, such as those based on lattice field theory.

Let us start by setting $N_{\mathrm{f}} = 0$ and varying N_{as}. A naíve estimate can be derived by taking the perturbative 2-loop beta function to hold beyond perturbation theory, using it to compute $N^{\mathrm{BZ,cr}}_{\mathrm{as}}$, and assuming that the fixed point disappears when $\alpha_{\mathrm{BZ}} \to \infty$, or equivalently by looking for solutions of the condition $b_2 \to 0$. Doing so yields $N^{\mathrm{BZ,cr}}_{\mathrm{as}} \simeq 3.7$ for $Sp(4)$. This approach can be systematically improved by including higher-order loops, up to $\ell_{\mathrm{max}} > 2$, in the expansion of the beta function $\beta(\alpha)$. One then seeks values of N_{as} for which $\alpha_{\mathrm{IR}} \to \infty$, with α_{IR} determined by solving $\beta(\alpha) \equiv -2\alpha \sum_{\ell=1}^{\ell_{\mathrm{max}}} b_\ell (\frac{\alpha}{4\pi})^\ell = 0$. In particular, one finds $N^{4-\mathrm{loop,cr}}_{\mathrm{as}} \simeq 4.1$ from the perturbative beta function at four loops in the $\overline{\mathrm{MS}}$-scheme [311]. It should be noted, however, that the results are affected by uncontrolled systematics, since the coefficients, b_ℓ, of the beta function, $\beta(\alpha)$, depend on the renormalization scheme at three or higher loops, when $\ell \geq 3$.

An alternative approach makes use of the Schwinger-Dyson (SD) equation in the ladder approximation, in which case conformality is assumed to be lost when $\alpha_{\mathrm{IR}} \equiv \alpha^{\mathrm{cr}}$, with $\alpha^{\mathrm{cr}} = \pi/3C_2(R)$, which yields $N^{\mathrm{SD}}_{\mathrm{as}} \simeq 6$ for $Sp(4)$. Going beyond the perturbative coupling expansion, a conjectured all-orders beta function $\beta^{\mathrm{all-orders}}(\alpha)$ [164], which involves the first two universal coefficients of $\beta(\alpha)$ and the anomalous dimension of fermion bilinear operator, $\gamma_{\bar\psi\psi}(\alpha)$, has been proposed.[3] In this case, the conformal window is determined by solving the condition $\beta^{\mathrm{all-orders}} = 0$ with the physical input for the value of $\gamma_{\bar\psi\psi}$ at

[3] A modified version of the all-orders beta function can also be found in Ref. [165].

the IR fixed point. For $\gamma_{\bar{\psi}\psi} = 1$, one finds $N_{\rm as}^{\text{all-orders, cr}} \simeq 5.5$ for $Sp(4)$.[4]

More recently, the scheme-independent BZ expansion in the small parameter $\Delta_{N_{\rm as}} = N_{\rm as}^{\rm AF} - N_{\rm as}^{\rm IR}$ has been extensively applied to the determination of physical quantities such as the anomalous dimension, $\gamma_{\bar{\psi}\psi}$, at the IR fixed point —see Ref. [176] and references therein. In Ref. [167], the authors determined the lower edge of the conformal window by imposing the critical condition of $\gamma_{\bar{\psi}\psi}(2 - \gamma_{\bar{\psi}\psi}) = 1$. This condition is identical to $\gamma_{\bar{\psi}\psi} = 1$ at infinite order, but displays better convergence at finite order in the $\Delta_{N_{\rm as}}$ expansion. The 4th order calculation yields $N_{\rm as}^{\gamma cc, \rm cr} \simeq 5.5$ for $Sp(4)$ [168].

These analytical approaches can be extended to determine the conformal window for the theory containing fermions in the multiple representations, $\{R_1, R_2, \ldots, R_k\}$, in which case the upper and lower bounds of the conformal window are described by $(k-1)$-dimensional hypersurfaces. For the $Sp(4)$ theories of interest with $N_{\rm f}$ Dirac fermions transforming in the fundamental and $N_{\rm as}$ in the 2-index antisymmetric representation, the results are summarized in Fig. 1.[5] The upper bound is determined by the condition $b_1(N_{\rm f}, N_{\rm as}) = 0$. The various alternative determinations of the lower bound are estimated as follows. The dashed line is obtained by setting $b_2(N_{\rm f}, N_{\rm as}) = 0$. The dot-dashed line corresponds to the result of the all-order beta function with the input of $\gamma_{\bar{\Psi}\Psi} = \gamma_{\bar{Q}Q} = 1$. The dotted and solid lines are the results of the SD analysis and the BZ expansion of $\gamma_{\bar{\Psi}\Psi}$ at the 3rd order in $\Delta_{N_{\rm f}(n_{\rm as})}$ [179] with the critical conditions applied to the antisymmetric fermions, $\alpha_{\rm BZ} = \alpha_{\rm as}^{\rm cr} = \pi/3C_2(\text{AS})$ and $\gamma_{\bar{\Psi}\Psi}(2 - \gamma_{\bar{\Psi}\Psi}) = 1$, respectively, as fermions in the higher representation are expected to condense first, resulting in the larger values of $\alpha^{\rm cr}$ and $\gamma_{\rm IR}$ [313]. It might be possible to make use of the five-loop computations in Refs. [169,170], to further improve these estimations of the conformal window, but this goes beyond the purposes of this discussion. For the purpose of phenomenological applications, the most interesting physical quantities one would like to determine within the conformal window are the anomalous dimensions of fermion bilinear operators (mesons) and chimera baryon operators. Perturbative calculations of the former are available in the literature, up to the 4th order of the coupling expansion [314,315] and at the 3rd order of the BZ expansion [179], while that of the latter is only available at the leading order in α [62]. All of these considerations, summarized in Fig. 1, offer some intuitive guidance for what can be expected, but non-perturbative instruments are needed to test these predictions and put Fig. 1 on firmer grounds.

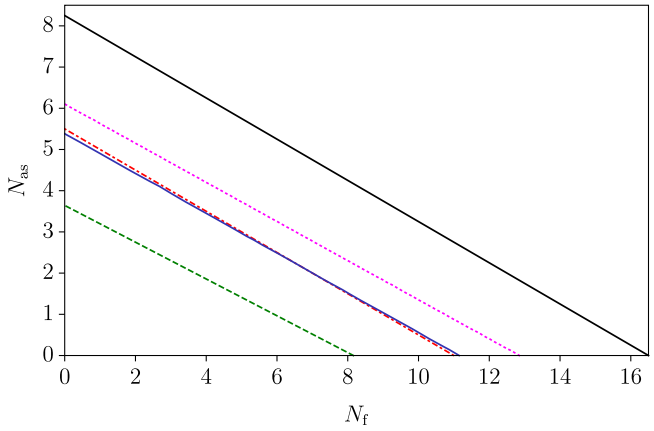

FIG. 1. Estimates of the extent of the conformal window in $Sp(4)$ theories coupled to $N_{\rm f}$ Dirac fermions transforming in the fundamental and $N_{\rm as}$ in the 2-index antisymmetric representation. The black solid line denotes the upper bound of the conformal window, while different colored and shaped lines denote alternative analytical estimates of the lower bound, obtained with different approximations. The dashed line is obtained by imposing the constraint $b_2(N_{\rm f}, N_{\rm as}) = 0$. The dot-dashed line is the result of the all-order beta function with the assumption that the anomalous dimensions of the fermion bilinears are $\gamma_{\bar{\Psi}\Psi} = \gamma_{\bar{Q}Q} = 1$. The dotted line is the result of the SD analysis. The BZ expansion leads to the lower (blue) solid line. Details about these approximations can be found in the main text and in the reference list.

B. The lattice theory

In presenting the lattice theory, we borrow again notation and conventions from Ref. [9]. The theory is defined on a Euclidean, hypercubic, four-dimensional lattice with spacing a, with L/a sites in the space directions and T/a in the time direction. The generic lattice site is denoted as x, and the link in direction μ as (x, μ). The total number of sites is thus $\tilde{V}/a^4 = T \times L^3/a^4$. Unless stated otherwise, in the following we set $L = T$. The action is the sum of two terms

$$S \equiv S_g + S_f, \tag{13}$$

where S_g and S_f are the gauge and fermion action, respectively. Among the several choices for the former—the Iwasaki, Symanzik, DBW2, and Wilson gauge actions —for simplicity, we show our results using the Wilson action, defined as

$$S_g \equiv \beta \sum_x \sum_{\mu<\nu} \left(1 - \frac{1}{2N} \text{Re Tr} \mathcal{P}_{\mu\nu}(x)\right), \tag{14}$$

[4]This choice for $\gamma_{\bar{\psi}\psi}$ has been argued to be the critical condition associated with the chiral phase transition through the IR and UV fixed point merger [182]., and by matching smoothly to the chiral phase with pions [310]. A less common choice is to set $\gamma_{\bar{\psi}\psi} = 2$, as suggested by unitarity considerations [312].

[5]The figure is basically the same as the analogous one found in Ref. [167], except that the input for the all-orders beta function analysis has been changed to $\gamma_{\bar{\Psi}\Psi} = \gamma_{\bar{Q}Q} = 1$. The parameter space has also been extended and the notation adapted to the conventions of this paper.

where $\mathcal{P}_{\mu\nu}(x) \equiv U_\mu(x)U_\nu(x+\hat{\mu})U_\mu^\dagger(x+\hat{\nu})U_\nu^\dagger(x)$ is known as the *elementary plaquette* operator, $U_\mu(x) \in Sp(2N)$ is the *link variable* defined on link (x,μ), and $\beta \equiv 4N/g_0^2$, where g_0 is the bare gauge coupling. For the fermions, we adopt the massive Wilson-Dirac action,

$$S_f \equiv a^4 \sum_{j=1}^{N_{\rm f}} \sum_x \bar{Q}^j(x) D_m^{(\rm f)} Q^j(x) + a^4 \sum_{j=1}^{N_{\rm as}} \sum_x \bar{\Psi}^j(x) D_m^{(\rm as)} \Psi^j(x), \tag{15}$$

where Q^j and Ψ^j are the fermion fields transforming, respectively, in the fundamental and 2-index antisymmetric representation and j is a flavor index, while color and spinor indices are omitted for simplicity. The massive Wilson-Dirac operators in Eq. (15) are defined as

$$D_m^{(\rm f)} Q^j(x) \equiv (4/a + m_0^{\rm f}) Q^j(x) - \frac{1}{2a} \sum_\mu \Big\{ (1-\gamma_\mu) U_\mu^{(\rm f)}(x) Q^j(x+\hat{\mu}) + (1+\gamma_\mu) U_\mu^{(\rm f),\dagger}(x-\hat{\mu}) Q^j(x-\hat{\mu}) \Big\}, \tag{16}$$

and

$$D_m^{(\rm as)} \Psi^j(x) \equiv (4/a + m_0^{\rm as}) \Psi^j(x) - \frac{1}{2a} \sum_\mu \Big\{ (1-\gamma_\mu) U_\mu^{(\rm as)}(x) \Psi^j(x+\hat{\mu}) + (1+\gamma_\mu) U_\mu^{(\rm as),\dagger}(x-\hat{\mu}) \Psi^j(x-\hat{\mu}) \Big\}, \tag{17}$$

where $m_0^{\rm f}$ and $m_0^{\rm as}$ are the bare fermion masses in the fundamental and 2-index antisymmetric representation, and $U_\mu^{(\rm f)}(x) = U_\mu(x)$. The link variables $U_\mu^{(\rm as)}(x)$ are defined as in Ref. [9], as follows:

$$U^{(\rm as)}_{\mu,(ab)(cd)} = \mathrm{Tr}(e^{(ab)T} U_\mu^{(\rm f)} e^{(cd)} U_\mu^{(\rm f)\rm T}), \tag{18}$$

where $e^{(ab)}$ are the elements of an orthonormal basis in the $(N(2N-1)-1)$-dimensional space of $2N \times 2N$ antisymmetric and Ω-traceless matrices, and the multi-indices (ab) run over the values $1 \le a < b \le 2N$. The entry ij of each element of the basis is defined as follows. For $b \neq N+a$,

$$e^{(ab)}_{ij} \equiv \frac{1}{\sqrt{2}} (\delta_{aj}\delta_{bi} - \delta_{ai}\delta_{bj}), \tag{19}$$

while for $b = N+a$ and $2 \le a \le N$,

$$e^{(ab)}_{i,i+N} = -e^{(ab)}_{i+N,i} \equiv \begin{cases} \frac{1}{\sqrt{2a(a-1)}}, & \text{for } i < a, \\ \frac{1-a}{\sqrt{2a(a-1)}}, & \text{for } i = a. \end{cases} \tag{20}$$

It is easy to verify that each element of this basis satisfies the Ω-traceless condition $\mathrm{Tr}(e^{(ab)}\Omega) = 0$, where the symplectic matrix Ω is defined in Eq. (A1).

Finally, we impose periodic boundary conditions on the lattice for the link variables, while for the fermions we impose periodic boundary conditions along the space-like directions, and anti-periodic boundary conditions along the time-like direction.

III. NUMERICAL IMPLEMENTATION: GRID

Our numerical studies are performed using Grid [292–294]: a high level, architecture-independent, C++ software library for lattice gauge theories. The portability of its single source-code across the many architectures that characterize the exascale platform landscape makes it an ideal tool for a long-term computational strategy. Grid has already been used to study theories based on $SU(N_c)$ gauge groups with $N_c \ge 3$, and fermions in multiple representations [316,317]. In this section, we describe the changes that have been implemented in Grid in order to enable the sampling of $Sp(2N)$ gauge field configurations. With the aim of including dynamical fermions in future explorations of $Sp(2N)$ gauge theories, we focused our efforts[6] on the Hybrid Monte Carlo (HMC) algorithm and on its variation, the rational HMC (RHMC), used whenever the number of fermion species is odd.

The (R)HMC algorithms generate a Markov chain of gauge configurations distributed as required by the lattice action described in Sec. II B. The ideas underpinning these two algorithms can be summarized as follows. Firstly, bosonic degrees of freedom ϕ and $\phi^\dagger$, known as pseudo-fermions, are introduced replacing a generic number n_f of fermions. Powers of the determinant of the hermitian Dirac operator, $Q_m^R = \gamma_5 D_m^R$, in representation R can then be expressed as

[6] An implementation of the Cabibbo-Marinari method [318] for pure gauge theories would be useful to explore general $Sp(2N)$ theories and extrapolate to the large-N_c limit. We postpone this task to future work.

$$(\det D_m^R)^{n_f} = (\det Q_m^R)^{n_f} = \int \mathcal{D}\phi\mathcal{D}\phi^\dagger e^{-a^4\sum_x \phi^\dagger(x)(Q_m^2)^{-n_f/2}\phi(x)}, \quad (21)$$

where flavor and color indices of ϕ and $\phi^\dagger$ have been suppressed for simplicity. For odd values of n_f, the rational approximation is used to compute odd powers of the determinant above, resulting in the RHMC.

Second, a fictitious classical system is defined, with canonical coordinates given by the elementary links and Lie-algebra-valued conjugate momenta $\pi(x,\mu) = \pi^a(x,\mu)t^a$, where t^a are the generators of the $\mathfrak{sp}(2N)$ algebra in the fundamental representation. The fictitious Hamiltonian is

$$H = \frac{1}{2}\sum_{x,\mu,a}\pi^a(x,\mu)\pi^a(x,\mu) + H_g + H_f, \quad (22)$$

where $H_g = S_g$ and $H_f = S_f$. The molecular dynamics (MD) evolution in fictitious time τ is dictated by

$$\frac{\mathrm{d}U_\mu(x)}{\mathrm{d}\tau} = \pi(x,\mu)U_\mu(x), \qquad \frac{\mathrm{d}\pi(x,\mu)}{\mathrm{d}\tau} = F(x,\mu), \quad (23)$$

where $F(x,\mu)$, known as the HMC force, is defined on the Lie algebra $\mathfrak{sp}(2N)$, and can be expressed as $F(x,\mu) = F_g(x,\mu) + F_f(x,\mu)$. The detailed form for $F_g(x,\mu)$ and $F_f(x,\mu)$ [191], the gauge and fermion force can be found in Sec. III A of Ref. [191].

Numerical integration of the MD equations thus leads to a new configuration of the gauge field, which is then accepted or rejected according to a Metropolis test. The update process can hence be described as follows:

(i) pseudofermions distributed according to the integrand in Eq. (21) are generated with the heat bath algorithm,
(ii) starting with Gaussian random conjugate momenta, the MD equations in Eq. (23) are integrated numerically,
(iii) the resulting gauge configuration is accepted or rejected by a Metropolis test.

In this section we provide details on the implementation of the operations listed above, focusing on the alterations made to the pre-existing structure of the code designed for $SU(N_c)$ gauge theories. We then describe and carry out three types of technical checks, following Ref. [191]. We test the behavior of the HMC and RHMC algorithms. We produce illustrative examples of the behavior of the molecular dynamics (MD). Finally, we carry out a comparison between HMC and RHMC algorithms. The purpose of these tests is to verify that the dynamics is implemented correctly.

A. Software development

As in the case for the preexisting routines handling the theories with gauge group $SU(N_c)$, our implementation of $Sp(2N)$ allows for a generic number of colors. The starting point of the MD is the generation of random Lie-algebra-valued conjugate momenta. The generators of the $\mathfrak{sp}(2N)$ Lie Algebra in the fundamental representation, as they appear in Grid, are provided by the relations described in Appendix B, where conventions for their normalization are also established. Generators in higher representations of the gauge group can be derived from the fundamental ones [191,316]. In particular, the generators of the algebra of $Sp(2N)$ in the antisymmetric representation can be obtained from the definition in Eq. (18), by Taylor expanding to first order around the unit transformation,

$$(t^a_{\mathrm{as}})_{(ab)(cd)} = \mathrm{Tr}(e^{(ab)T}t^a_{\mathrm{f}}e^{(cd)} + e^{(ab)T}e^{(cd)}t^{aT}_{\mathrm{f}}). \quad (24)$$

In the numerical integration of Eq. (23), it is required to project the HMC force on the Lie algebra of the gauge group. In Grid, the embedding of the force-projection within the integrator requires the forces to be anti-Hermitian. Hence, a projection operation to the matrices of the algebra $\mathfrak{sp}(2N)$ must be defined. This can be done in analogy with the projection to $\mathfrak{su}(N_c)$, defined for a generic matrix M as

$$P_{\mathrm{tr}}P_{\mathrm{aH}}M, \quad (25)$$

where $P_{\mathrm{tr}}M \equiv M - \mathbb{1}_{N_c}\mathrm{Tr}(M)/N_c$ and $P_{\mathrm{aH}}M \equiv (M - M^\dagger)/2$ are the projectors to its traceless and to its anti-Hermitian parts, respectively. For $\mathfrak{sp}(2N)$, the projection is instead defined as,

$$P_{\mathrm{aH}}P^-_{\mathrm{Sp}}P_{\mathrm{tr}}M, \quad (26)$$

where

$$P^\pm_{\mathrm{Sp}}M \equiv \frac{M \pm \Omega M^*\Omega}{2}. \quad (27)$$

Notice that P^-_{Sp} returns an anti-Hermitian matrix, while P^+_{Sp} projects on a space of Hermitian matrices.

The resympleticization of gauge links to the $Sp(2N)$ group manifold has also been implemented in Grid. The algorithm [1] is a modification of the Gram-Schmidt process designed to take into account the condition in Eq. (A3). After normalizing the first column of the matrix U, the $(N+1)$-th column is set to

$$\mathrm{col}(U)_{j+N} = -\Omega\mathrm{col}(U)^*_j. \quad (28)$$

The second column is then obtained by orthonormalization with respect to both the first and the $N+1$-th column. An iteration of this process leads to a $Sp(2N)$ matrix. This procedure, performed after every update, prevents the gauge fields from drifting away from the group manifold due to the finite precision of the simulation.

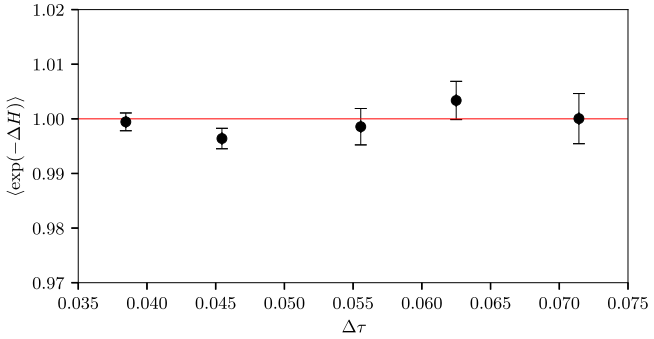

FIG. 2. Test of Creutz equality, $\langle \exp(-\Delta H)\rangle = 1$; dependence of $\langle \exp(-\Delta H)\rangle$ on the time–step $\Delta\tau$ in the MD integration, for $N = 2$, $N_{\rm f} = 0$, and $N_{\rm as} = 4$. The relevant parameters of this study are the trajectory length $\tau = 1$, number of steps $n_{\rm steps} = 14$, 16, 18, 22, 26 ($\Delta\tau = \tau/n_{\rm steps}$), for an ensemble with lattice volume $\tilde{V}/a^4 = 8^4$, $\beta = 6.8$, and $am_0^{\rm as} = -0.6$.

B. Basic tests of the algorithm

In this subsection, we follow closely Secs. III and IV of Ref. [191]. Our MD evolution is implemented using a second-order Omelyan integrator [319]. However, in this work, the inversion of the fermion matrix is treated without preconditioning [9,320].

We now restrict attention to the theory with $N = 2$, $N_{\rm f} = 0$, and $N_{\rm as} = 4$, and perform a set of preliminary checks on the algorithms we use. We present the results in Figs. 2–6, obtained, for convenience, setting the lattice parameters to $\beta = 6.8$, and $am_0 = -0.6$, on an isotropic lattice with volume $\tilde{V} = (8a)^4$.

The first test pertains to Creutz equality [321]: by measuring the difference in Hamiltonian, ΔH, evaluated before and after the MD evolution, one should find that

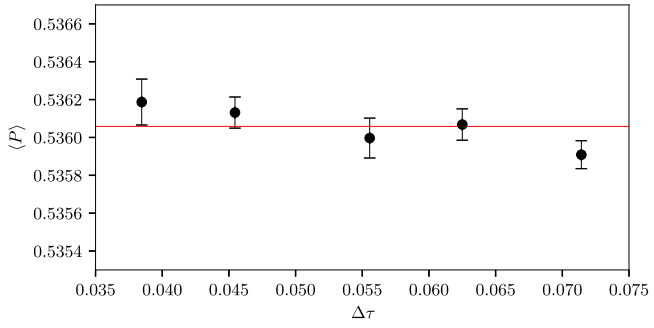

FIG. 3. Test of independence of the plaquette on the time–step $\Delta\tau$ used for the MD integration, for $N = 2$, $N_{\rm f} = 0$, and $N_{\rm as} = 4$. The relevant parameters of this study are the trajectory length $\tau = 1$, number of steps $n_{\rm steps} = 14$, 16, 18, 22, 26, $\Delta\tau = \tau/n_{\rm steps}$, for an ensemble with lattice volume $\tilde{V}/a^4 = 8^4$, $\beta = 6.8$, and $am_0^{\rm as} = -0.6$. The horizontal line corresponds to the plaquette value obtained averaging over trajectories having different a number of step values, $n_{\rm steps}$.

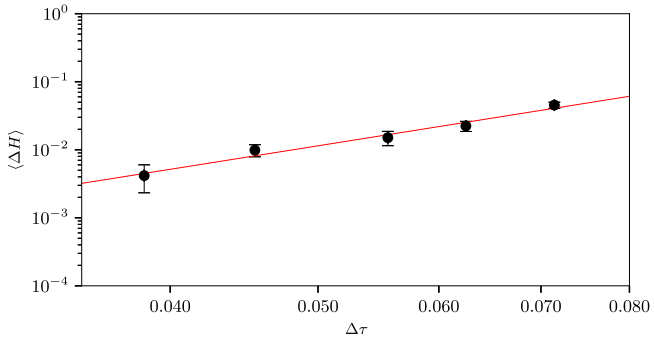

FIG. 4. Dependence of $\langle \Delta H\rangle$ on the time-step, $\Delta\tau$, used for the MD integration, for $N = 2$, $N_{\rm f} = 0$, and $N_{\rm as} = 4$. The expectation value $\langle \Delta H\rangle$ is proportional to $(\Delta\tau)^4$, consistently with the use of a second-order integrator. The plot is shown in log-log scale. The relevant parameters of this study are the trajectory length $\tau = 1$, number of steps $n_{\rm steps} = 14, 16, 18, 22, 26$ ($\Delta\tau = \tau/n_{\rm steps}$), for an ensemble with lattice volume $\tilde{V}/a^4 = 8^4$, $\beta = 6.8$, and $am_0 = -0.6$.

$$\langle \exp\left(-\Delta H\right)\rangle = 1. \tag{29}$$

This is supported by our numerical results: Fig. 2 shows the value of $\langle \exp(-\Delta H)\rangle$ for five different choices of the time-step used in the MD integration, with $\Delta\tau = \tau/n_{\rm steps}$, and the choice $\tau = 1$. The numerical results are obtained by considering a thermalized ensemble consisting of 3400 trajectories, that we find has integrated autocorrelation time $\tau_c = 6.1(2)$, measured using the Madras-Sokal windowing process [322]. A closely related test is shown in Fig. 3: the value of the ensemble average of the plaquette is independent of $\Delta\tau$.

A third test pertains to the dependence of $\langle \Delta H\rangle$ on $\Delta\tau$, which for a second-order integrator is supposed to scale as $\langle \Delta H\rangle \propto (\Delta\tau)^4$ [323]. In Fig. 4 we show our measurements,

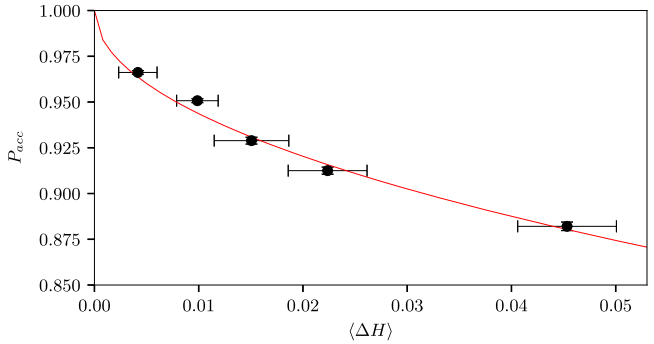

FIG. 5. Test of the relation between acceptance probability and ΔH, for $N = 2$, $N_{\rm f} = 0$, and $N_{\rm as} = 4$. The expected behavior $P_{acc} = erfc(\sqrt{\Delta H}/2)$ is supported. The relevant parameters of this study are the trajectory length $\tau = 1$, number of steps $n_{\rm steps} = 14, 16, 18, 22, 26$ ($\Delta\tau = \tau/n_{\rm steps}$), for an ensemble with lattice volume $\tilde{V}/a^4 = 8^4$, $\beta = 6.8$, and $am_0 = -0.6$.

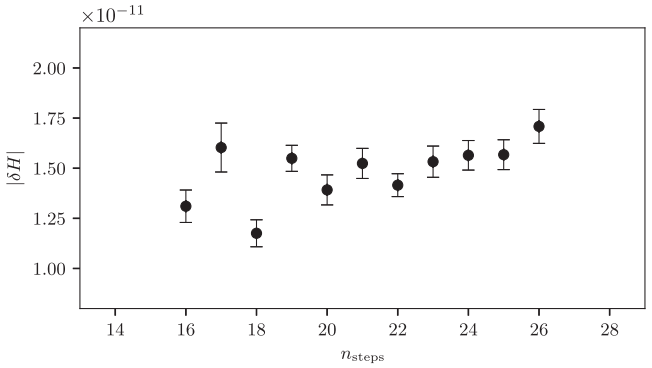

FIG. 6. Reversibility test, showing $|\delta H|$ for various choices of $\Delta\tau$, for $N = 2$, $N_f = 0$, and $N_{as} = 4$. The relevant parameters of this study are the trajectory length $\tau = 1$, number of steps $n_{steps} \in [16, 26]$ ($\Delta\tau = \tau/n_{steps}$), for an ensemble with lattice volume $\tilde{V}/a^4 = 8^4$, $\beta = 6.8$, and $am_0 = -0.6$.

together with the result of a best-fit to the curve $\log\langle\Delta H\rangle = \mathcal{K}_1 \log(\Delta\tau) + \mathcal{K}_2$, with $\mathcal{K}_1 = 3.6(4)$ determined by minimizing a simple χ^2. We find good agreement, as quantified by the value of the reduced $\chi^2/N_{d.o.f.} = 0.6$, and $\mathcal{K}_1$ is compatible to 4. A closely related test is displayed in Fig. 5, confirming the prediction that the acceptance probability of the algorithm, P_{acc}, obeys the relation [324]:

$$P_{acc} = \mathrm{erfc}\left(\frac{1}{2}\sqrt{\langle\Delta H\rangle}\right). \tag{30}$$

The final test of this subsection is displayed in Fig. 6. We refer the reader to Refs. [191,325], for discussions, rather than reproduce them here. Following Refs. [191,325], we also want to ensure that the reversibility of our updates is respected. Reversibility is one of the fundamental properties required in order to pursue a correct HMC update. Our update algorithm, based on leapfrog, is reversible analytically. Yet, when using this algorithm numerically on computers, because of the finite precision, exact reversibility is lost. It is therefore important to verify that implementation of the fundamental steps of the algorithm can be considered as reversible to good approximation, in order to avoid that rounding errors introduce a significant bias in our calculations. One can show that the quantity $|\delta H|$—the average difference of the Hamiltonian evaluated by evolving the MD forward and backward and flipping the momenta at $\tau = 1$—does not change significantly in our simulations. Since the Hamiltonian in these tests is of order $\sim 10^6$ and the typical $\delta H \sim 10^{-11}$, the results show that the violation of reversibility is consistent with having $|\delta H|/H$ of the order of the numerical accuracy. This is the expected relative precision for double-precision floating-point numbers. Moreover, the violation $|\delta H|$ is independent of $\Delta\tau$. As a "microscopic" and related effect, reversibility violations may occur while updating the gauge link variables and momenta updates during the MD evolution. To ensure this does not occur we update the gauge links through the exponentiation of the momenta, so that $U(\pi)U(-\pi) = 1$.

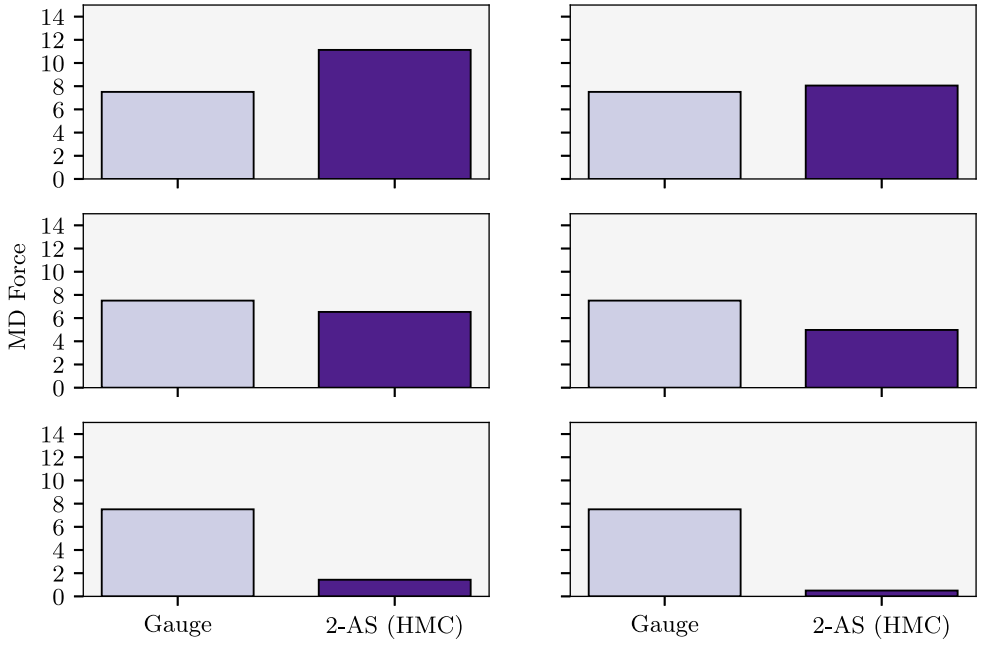

FIG. 7. Field contribution to the MD force for the theory with $N = 2$, $N_f = 0$, and $N_{as} = 4$, on isotropic lattice with $\tilde{V} = (8a)^4$, and lattice coupling $\beta = 6.8$. The two blocks are respectively indicating the gauge (light shading, left) and the fermion (dark shading, right) contribution, the latter computed with the HMC algorithm. Fermion contributions are summed over flavor. The six panels correspond to different choices of bare mass: $am_0^{as} = -0.9, -0.1, +0.6, +1.8, +15, +50$ (left to right, top to bottom).

Moreover, thanks to the double-precision nature of the variables we use, the entity of relative violations for momenta results to be within machine-accuracy in our simulations, as in the global reversibility violation case.

C. More about the molecular dynamics

For illustration purposes, we find it useful to monitor the contribution to the MD of the fields, and how this changes as we dial the lattice parameters. We focus on the theory with $N = 2$, $N_f = 0$, and $N_{as} = 4$, and consider a few ensembles with isotropic lattice with $\tilde{V} = (8a)^4$, and lattice coupling $\beta = 6.8$, but vary the mass am_0^{as}. We show in Fig. 7 the force, F, as defined in Eq. (23), split in its contribution from the gauge and fermion dynamics, the latter computed using the HMC for all fermions. The results are normalized so that the gauge contribution is held constant. As can be clearly appreciated, for large and positive values of am_0^{as} the fermions can be neglected, as for these choices of the mass, one expects to be in the quenched regime. When decreasing the mass, the fermion contribution increases. For large, negative values of the Wilson bare mass (close to the chiral limit), the fermion contribution is even larger than the contribution of the gauge part of the action.

D. Comparing HMC and RHMC

While in this paper we are mostly interested in the theory with $N = 2$, $N_f = 0$, and $N_{as} = 4$, and hence we can use the HMC algorithm, for the general purpose of identifying the extent of the conformal window in this class of lattice gauge theories it may be necessary to consider also odd numbers of fermions, for which we resort to the RHMC algorithm. The latter relies on a rational approximation in the computation of the fermion force, but the presence of a Metropolis accept-reject step ensures that the algorithm is exact. Thus, a preliminary test must be made to check the consistency of the implementation—as was done for $SU(3)$ theories, see for instance Ref. [326].[7] To gauge whether the numerical implementation is working at the desired level of accuracy and precision, we performed the exercise leading to Fig. 8. We computed the average plaquette, $\langle P \rangle$, where P is defined as

$$P \equiv \frac{a^4}{6\tilde{V}} \sum_x \sum_{\mu<\nu} \left[\frac{1}{2N} \mathrm{Re}\,\mathrm{Tr} \mathcal{P}_{\mu\nu}(x) \right] \tag{31}$$

for ensembles having lattice volume $\tilde{V} = (8a)^4$ and coupling $\beta = 6.8$, for a few representative choices of the bare mass $-1.4 \leq am_0^{as} \leq 0.0$. We repeated this exercise three times: at first, we treated all fermions with the HMC, then we treated them all with the RHMC, and finally we used a mixed strategy, treating two fermions with the HMC, and two with the RHMC. We display, in the two plots in the figure, the differences of the second and third approaches to the first one, respectively. We detect no visible discrepancies. For most of the data, the differences are compatible with zero within the statistical uncertainties. More generally, given the number of observables, the probability to find a deviation larger than 3σ from the null value results to be $\sim 12\%$.

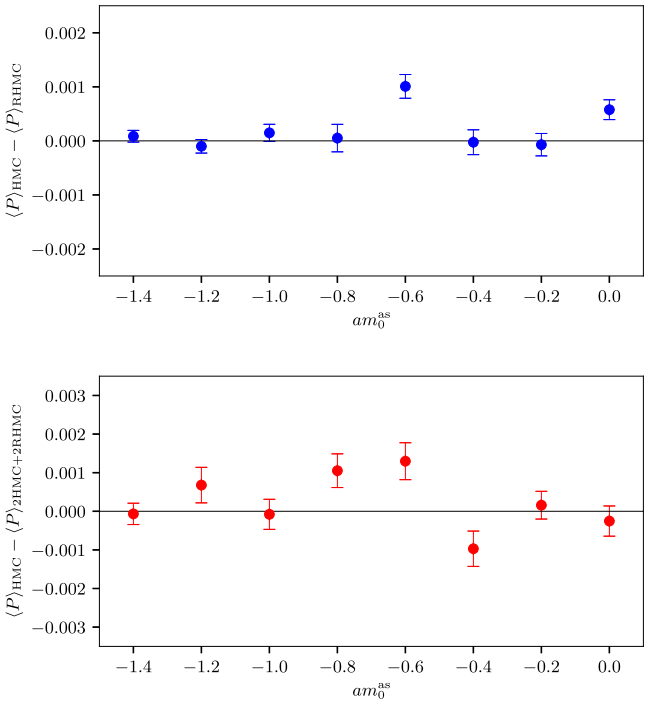

FIG. 8. Compatibility between plaquette averages $\langle P \rangle$ obtained with HMC and RHMC algorithms for the theory with $N = 2$, $N_f = 0$, and $N_{as} = 4$. $\langle P \rangle_{\mathrm{HMC}}$ is obtained running two couples of fermions with HMC. For $\langle P \rangle_{\mathrm{RHMC}}$ (top panel), RHMC was applied individually to each of the fermions. $\langle P \rangle_{\mathrm{2HMC+2RHMC}}$ (bottom panel) is obtained running two fermions with HMC, while the other two were run with RHMC. The lattice coupling is $\beta = 6.8$, with the bare mass in the range $-1.4 \leq am_0^{as} \leq 0.0$. The lattice is isotropic and has volume $\tilde{V} = (8a)^4$.

IV. THE $N = 2$ LATTICE YANG-MILLS THEORY

In this section, we start to analyse the physics of the $Sp(4)$ theory of interest. We begin from the pure Yang-Mills dynamics, with $N_f = 0 = N_{as}$. We verify that center symmetry, $(\mathbb{Z}_2)^4$, is broken at small volumes, but restored at large volumes, by looking at the (real) Polyakov loop, in a way that is reminiscent of Ref. [218]. Following Ref. [316], we then consider the spectrum of the Dirac operator in the quenched approximation, both for

[7] We note that to check the correctness of the Remez implementation, one could in principle use any function of an arbitrary matrix M. In particular, choosing diagonal matrices would make the comparison straightforward. Grid makes use of this methodology in its test suite.

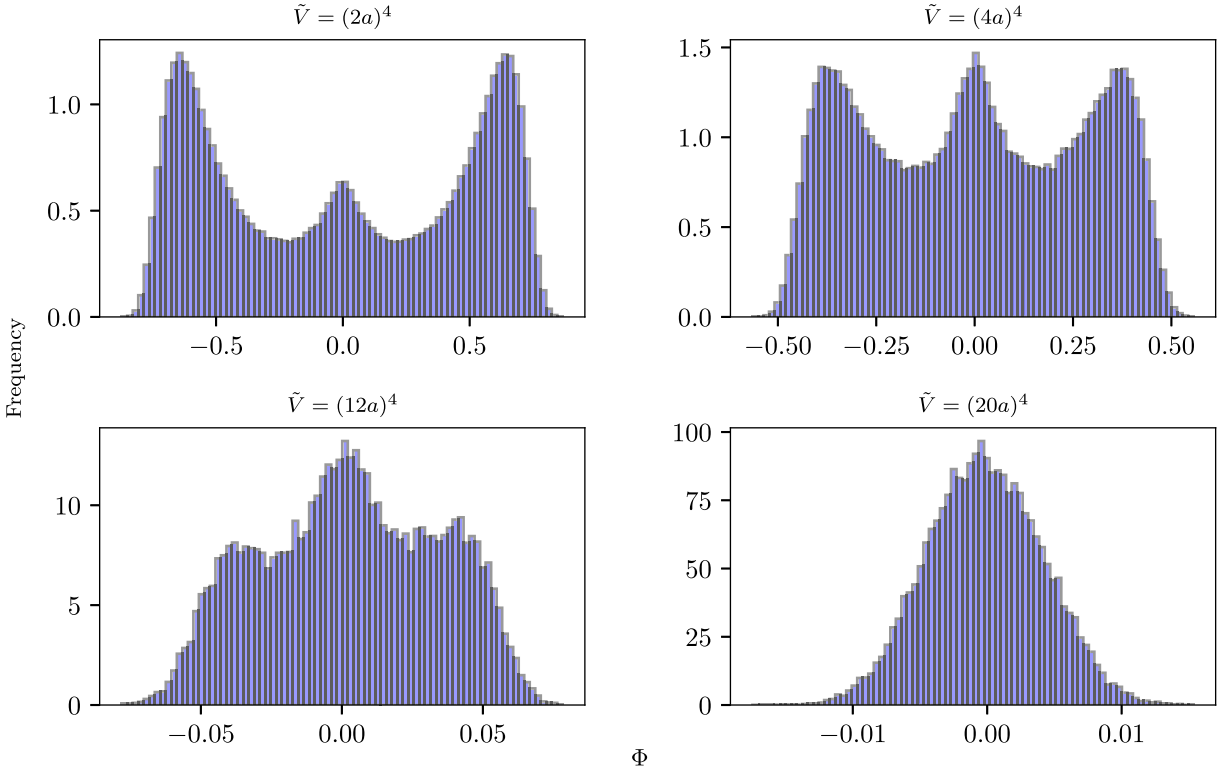

FIG. 9. Study of finite-size effects on the lattice, for the $Sp(4)$ Yang-Mills theory. The histograms depict the distribution of (real) Polyakov loops for ensembles with $\beta = 9.0$ and four choices of space-time volume: $\tilde{V} = (2a)^4, (4a)^4, (12a)^4, (20a)^4$. The histograms' areas are normalized to 1.

fundamental and 2-index antisymmetric fermions, to verify the symmetry-breaking pattern expected from random matrix theory.

The results for the first of these tests are shown in Fig. 9. At a coupling $\beta = 9.0$, we generate four ensembles in the pure $Sp(4)$ theory, at different values of the space-time volume, $\tilde{V} = (2a)^4, (4a)^4, (12a)^4, (20a)^4$. For each configuration, we compute the spatial averaged (real) Polyakov loop, defined as

$$\Phi \equiv \frac{1}{N_c N_s^3} \sum_{\vec{x}} \mathrm{Tr}\left(\prod_{t=0}^{t=N_t-1} U_0(t, \vec{x}) \right), \tag{32}$$

where $U_0(t, \vec{x})$ is the time-like link variable. For our current purposes, we choose the lattice to be isotropic in all four directions, $N_t = N_s = L/a$. For each ensemble, we display the frequency histogram of the values of Φ. The expectation is that the zero-temperature $Sp(4)$ lattice theory should preserve the $(\mathbb{Z}_2)^4$ symmetry of the center of the group in four Euclidean space-time dimensions. This is indeed the case for sufficiently large volumes, as shown by the bottom-right panel of Fig. 9, for which $N_t = N_s = 20$, that exhibits a Gaussian distribution centred at the origin. But for small enough lattice volumes, this expectation is violated. This is visible in the other three panels in Fig. 9, in which the distribution is non-Gaussian, and two other peaks emerge. In the extreme case of $N_s = N_t = 2$, the two peaks at finite value of Φ dominate the distribution, which is otherwise symmetrical around zero. Interestingly, Polyakov loops can be used also to perform the more physical study of the finite-temperature confinement/deconfinement phase transition. In this case, one would consider $N_t \neq N_s$, vary the coupling β to identify the transition temperature, and then perform continuum and infinite volume extrapolations. The characterization of the deconfinement phase transition is of interest for both theoretical as well as phenomenological reasons—see Ref. [156] and the review in Ref. [19]—but requires a dedicated, extensive programme of numerical work, and possibly cutting-edge new technology to address some of the difficulties faced by conventional Monte Carlo sampling methods (see, e.g., the discussions in Refs. [327,328]), while the simpler analysis performed here suffices for the more modest purposes of this paper.

Ensembles of gauge configurations without dynamical fermions can also be used to verify that our implementation of the Dirac operators is correct. To this purpose, following Ref. [316] (and Ref. [9]), we consider the theory with quenched fermions in either the fundamental or 2-index antisymmetric representation, and compute the spectrum of eigenvalues of the Hermitian Wilson-Dirac operator $Q_m = \gamma_5 D_m$. The numbers of configurations are $N_{\mathrm{conf,f}} = 88$ and $N_{\mathrm{conf,as}} = 47$, while the number of eigenvalues in

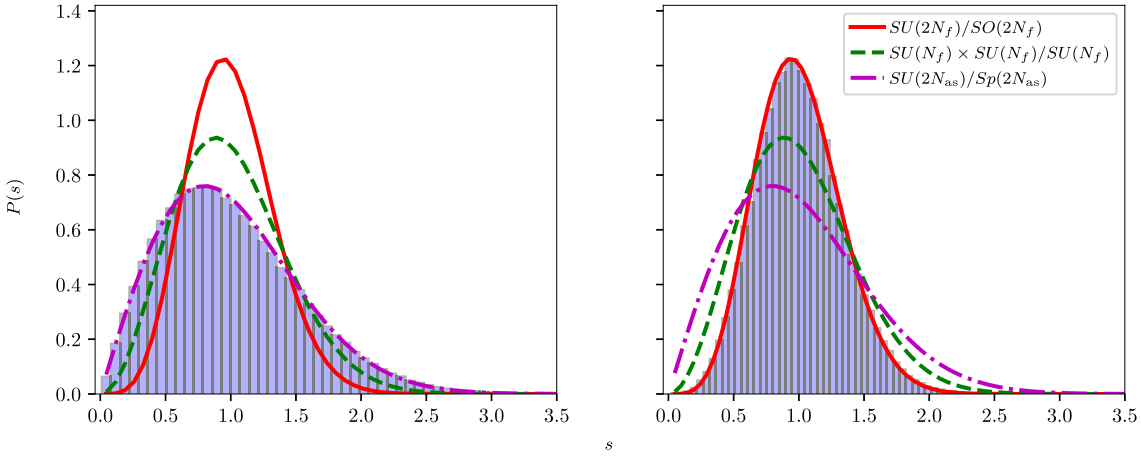

FIG. 10. Distribution of the folded density of spacing between subsequent eigenvalues of the hermitian Dirac-Wilson operator $Q_m = \gamma_5 D_m$, and comparison with predictions from chRMT, computed in the quenched approximation, with ensembles having $\beta = 8.0$, $am_0 = -0.2$, and lattice volume $\tilde{V} = (4a)^4$, in the $Sp(4)$ theory. The left panel shows the case of fermions transforming in the fundamental representation, and the right is for fermions in the 2-index antisymmetric one.

each configuration used is 3696 for fundamental fermions and 5120 for antisymmetric fermions. Then, we compute the distribution of the folded density of spacing, $P(s)$. Finally, we compare the results to the exact predictions of chiral random matrix theory (chRMT) [329,330]. Because the spectrum captures the properties of the theory, in particular the pattern of chiral symmetry breaking [331], the distribution $P(s)$ differs, depending on the symmetry-breaking pattern predicted. The folded density of spacing is

$$P(s) = N_{\tilde{\beta}} s^{\tilde{\beta}} \exp\left(-c_{\tilde{\beta}} s^2\right), \quad \text{where}$$
$$N_{\tilde{\beta}} = 2\frac{\Gamma^{\tilde{\beta}+1}\left(\frac{\tilde{\beta}}{2}+1\right)}{\Gamma^{\tilde{\beta}+2}\left(\frac{\tilde{\beta}+1}{2}\right)}, \qquad c_{\tilde{\beta}} = \frac{\Gamma^2\left(\frac{\tilde{\beta}}{2}+1\right)}{\Gamma^2\left(\frac{\tilde{\beta}+1}{2}\right)}, \tag{33}$$

where $\tilde{\beta}$ is the Dyson index. This index can take three different values: $\tilde{\beta} = 2$ corresponds to the symmetry breaking pattern $SU(N_f) \times SU(N_f) \to SU(N_f)$, $\tilde{\beta} = 1$ to $SU(2N_f) \to Sp(2N_f)$, $\tilde{\beta} = 2$ corresponds to the symmetry breaking pattern $SU(N_f) \times SU(N_f) \to SU(N_f)$ and $\tilde{\beta} = 4$ to $SU(2N_f) \to SO(2N_f)$. The latter two are the cases we are interested in, corresponding to fundamental and 2-index antisymmetric fermions for the symplectic theory.

In order to make a comparison with the chRMT prediction in Eq. (33), we compute the eigenvalues of Q_m for N_{conf} configurations. This process yields a set of eigenvalues $\lambda_i^{(c)}$ with $c = 1, \ldots, N_{\text{conf}}$. The eigenvalues are arranged in one long list, in which $\lambda_i^{(c)}$ are ordered in ascending order. Any degeneracy that is present in the 2-antisymmetric case is discarded. Then, for each $c = 1, \ldots, N_{\text{conf}}$, a new list of values is produced, that contains $n_i^{(c)}$, the positive integer position of the eigenvalue $\lambda_i^{(c)}$ in the long list ordered in ascending order, instead of $\lambda_i^{(c)}$. The density of spacing, s, is replaced by the expression

$$s = \frac{n_{i+1}^{(c)} - n_i^{(c)}}{\mathcal{N}}. \tag{34}$$

The constant $\mathcal{N}$ is defined so that the density of spacing has unit average over the whole ensemble, $\langle s \rangle = 1$. Finally, the (discretized) unfolded density of spacings, $P(s)$, is obtained by binning numerical results for s and normalizing it.

In Fig. 10, we show an example of the folded distribution of eigenvalues of the Wilson-Dirac operator, computed numerically. As it can be seen, in the case of fermions in the fundamental representation, one finds a distribution that is compatible with the symmetry breaking pattern leading to the coset $SU(2N_f)/Sp(2N_f)$. Conversely, for fermions in the 2-index antisymmetric representation, our numerical results reproduce the prediction associated with the coset $SU(2N_{as})/SO(2N_{as})$. The spectacular agreement with chRMT confirms that there are no inconsistencies in our way of treating fermions. The size of the lattices we have considered has been chosen in order to make finite-size effects negligible reduce finite-size effects. These effects, as shown in Ref. [9], can become evident in smaller lattices and they lead to discrepancies due to some abnormally large spacings for the smallest and largest eigenvalues. This was interpreted to be an artefact due to the finiteness of the lattice size. We observe that, as in previous studies, the antisymmetric representation already matches the predictions in a 4^4 volume, while for the fundamental to

reproduce the predictions chRMT, we had to remove the 200 lowest and highest eigenvalues (reducing the number of eigenvalues from 4096 to 3696). In this fashion, the differences with chRMT are no longer visible to the naked eye even for lattices with modest volume, $\tilde{V} = (4a)^4$.

V. THE $N = 2$ THEORIES COUPLED TO FERMIONS: BULK PHASE STRUCTURE

In this section, we present our main results for the theory with $N = 2$, $N_f = 0$, and varying number of fermions transforming in the antisymmetric representation, starting from $N_{as} = 4$—for which we apply the HMC algorithm. We performed a coarse scan of the lattice parameter space, to identify phase transitions in the (β, m_0) plane, by studying the average plaquette, $\langle P \rangle$, its hysteresis, and its susceptibility. We provide an approximate estimate of the upper bound coupling for the bulk phase, β_*, above which there is no bulk phase transition, and hence one can safely perform lattice numerical calculations at finite lattice spacing, yet confident that the results can be extrapolated to the appropriate continuum limit.

Figure 11 displays the average plaquette, $\langle P \rangle$, obtained in ensembles generated using a cold start. The lattice size is $\hat{V} = (8a)^4$, and each point is obtained by varying the lattice coupling $\beta = 7.0, 6.8, 6.6, 6.5, 6.4, 6.3, 6.2, 6.0, 5.8, 5.6$ and the bare mass $-1.4 \leq am_0^{as} \leq 0.0$. The figure shows that, for small values of β and large, negative values of the bare mass, the average plaquette displays an abrupt change at a particular value am_0^{as*}, while being a smooth, continuous function elsewhere. This is a first indication of the existence of a first-order bulk phase transition.

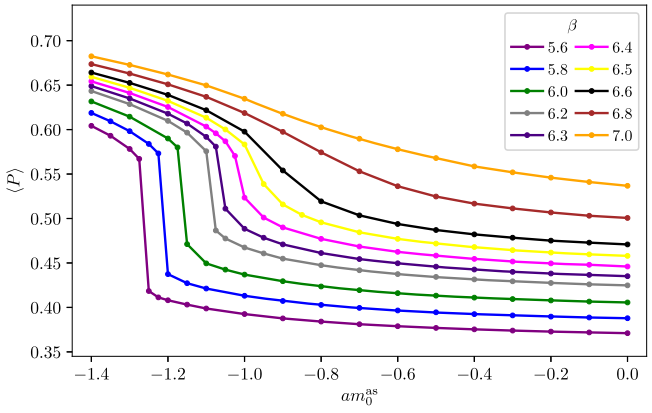

FIG. 11. Parameter scan of the $Sp(4)$ theory with $N_{as} = 4$ fermions transforming in the 2-index antisymmetric representation, with ensembles generated from a cold start, using the HMC. We show the value of the average plaquette, $\langle P \rangle$, as a function of the bare mass, for a few representative values of the coupling. The lattice size is $\tilde{V} = (8a)^4$, and each point is obtained by varying the lattice coupling $\beta = 7.0, 6.8, 6.6, 6.5, 6.4, 6.3, 6.2, 6.0, 5.8, 5.6$ and the bare mass $-1.4 \leq am_0^{as} \leq 0.0$.

To better understand whether a first-order phase transition is taking place, we study the effect of adopting two different strategies in the generation of the ensembles, repeating it using of thermalized (hot) starts, and redoing the measurements. Figure 12 shows the comparison of the average plaquette, $\langle P \rangle$, computed for several fixed choices of the coupling β, while varying the bare mass $-1.4 \leq am_0^{as} \leq 0.0$. The two curves in the plots represent the behavior measured in ensembles obtained from a cold and hot start configuration. The effects of hysteresis are clearly visible for $\beta < 6.4$ and are an indication of the presence of a first-order phase transition taking place at a critical value of the bare mass am_0^{as*}.

The final test of the nature of the phase transition is shown in Fig. 13. For illustration purposes, we choose two values of the coupling for which we have evidence of a phase transition ($\beta = 6.2$), or of smooth behavior of $\langle P \rangle$ for all value of am_0^{as} ($\beta = 6.5$), respectively. We compute the plaquette susceptibility, defined as

$$\chi_P \equiv \frac{\tilde{V}}{a^4}(\langle P^2 \rangle - (\langle P \rangle)^2), \tag{35}$$

and compare the numerical results obtained with ensembles having two different volumes, $\tilde{V} = (8a)^4$ and $\tilde{V} = (16a)^4$. The results indicate that the peak height scales as the 4-volume when β is small, in which case the position of the peak also moves to a different value of am_0^{as}. These are indeed the expected signature of a first order phase transition. For large β, the curved obtained for different volumes are compatible with one another,we observe a shift in values of am_0^{as} and no clear and large change in entity for the peak heights between the two volumes. This is a clear indication of a smooth crossover. We hence conclude that, in the theory with $N = 2$, $N_f = 0$, and $N_{as} = 4$, there is numerical evidence of a line of first-order phase transitions turning into a crossover at $\beta > \beta_* = 6.4$.

A. Varying N_{as}

We repeat the parameter scan for other choices of N_{as}, using the RHMC for all fermions when N_{as} is odd, and the HMC algorithm otherwise. The purpose of the exercise is to study the dependence of the upper bound coupling for the bulk phase β_* on the number of fermions, N_{as}. Indeed, it is expected that for small N_{as} we expect the theory to confine, while for larger values of $N_{as} \sim N_{as}^c$ the theory should approach the lower end of the conformal window, and eventually lose asymptotic freedom—we recall that the latter requires to impose the bound $N_{as} < 33/4$ in $Sp(4)$, while setting the stage for a first truly nonperturbative determination of the former is the main motivation for this study.

The results of these studies are shown in Fig. 14, which displays our measurements of the average plaquette, $\langle P \rangle$, as

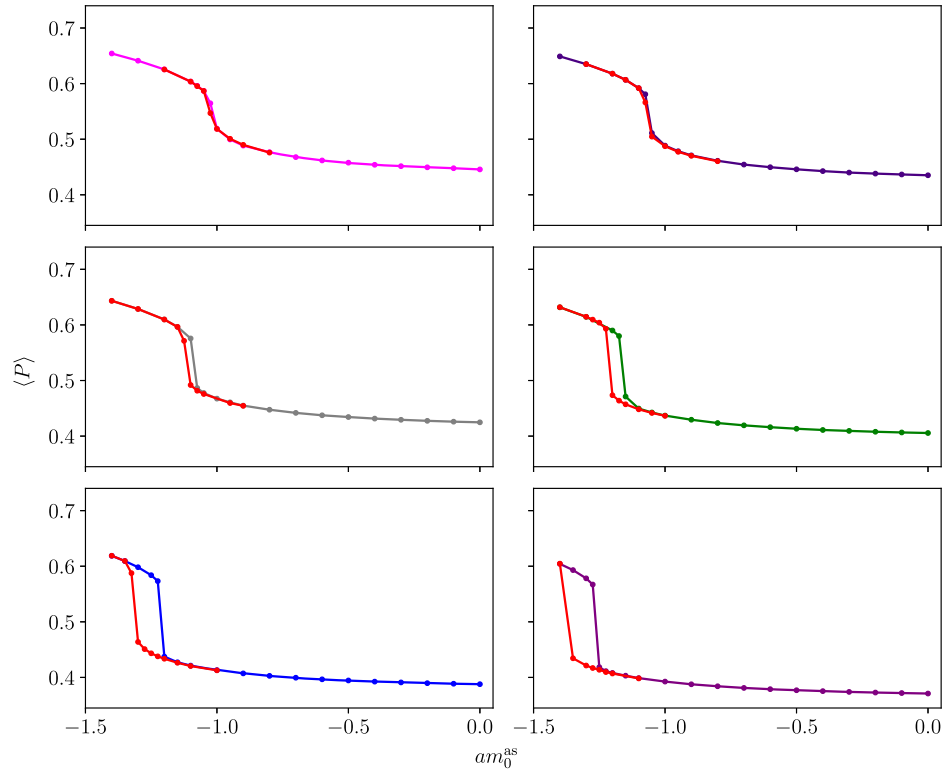

FIG. 12. Hysteresis between hot (red) and cold (other colors) starts for the $Sp(4)$ theory with $N_{\rm as} = 4$ fermions in the 2-index antisymmetric representation. The lattice coupling is $\beta = 6.4, 6.3, 6.2, 6.0, 5.8, 5.6$ (left to right, and top to bottom). The lattice size is $\tilde{V} = (8a)^4$, and each point is obtained by varying the bare mass $-1.4 \leq am_0^{\rm as} \leq 0.0$.

a function of the bare parameters of the theories. For the pure gauge $Sp(4)$ theory, we get plaquette values that are in agreement with the ones shown in Ref. [156]. The corresponding upper bound value of the coupling is roughly estimated to be $\beta_* \simeq 7.2$.

For theories with dynamical fermions, we vary both the masses and the coupling of the theories. As can be seen from Fig 14, for $N_{\rm as} = 1$ the upper bound is $\beta_* \simeq 6.7$. For $N_{\rm as} = 2$ the upper bound is $\beta_* \simeq 6.7$, and for $N_{\rm as} = 3$ it is $\beta_* \simeq 6.5$, in agreement with the values found in Ref. [2].

At a larger number of fermions species, we obtain progressively smaller values of β for the upper bound of the bulk phase β: for $N_{\rm as} = 5$, we get $\beta_* \simeq 6.3$. For $N_{\rm as} = 6$, the upper bound coupling is $\beta_* \simeq 6.2$. For $N_{\rm as} = 7$, we get $\beta_* \simeq 6.1 \div 6.2$ and for $N_{\rm as} = 8$, $\beta_* \simeq 6.1$. Overall, we notice a trend according to which the more fermion flavors are present in the $Sp(4)$, the smaller the upper bound value of the coupling we find and the bigger is the corresponding critical bare mass $am_0^{({\rm as})*}$.

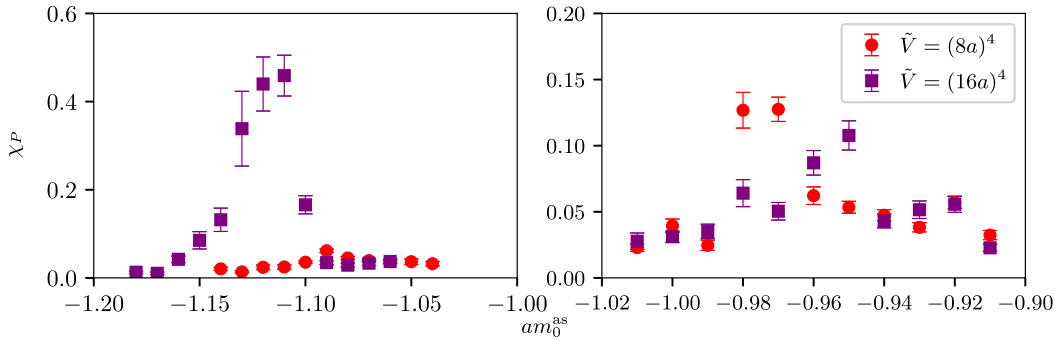

FIG. 13. Plaquette susceptibility, χ_P, in the $Sp(4)$ lattice theory with $N_{\rm as} = 4$ fermions in the 2-index antisymmetric representation. We use two values of the lattice size, $\tilde{V} = (8a)^4$ and $\tilde{V} = (16a)^4$. The ensembles have $\beta = 6.2$, $-1.18 \leq am_0 \leq -1.04$ (left panel), and $\beta = 6.5$, $-1.01 \leq am_0 \leq -0.91$ (right panel).

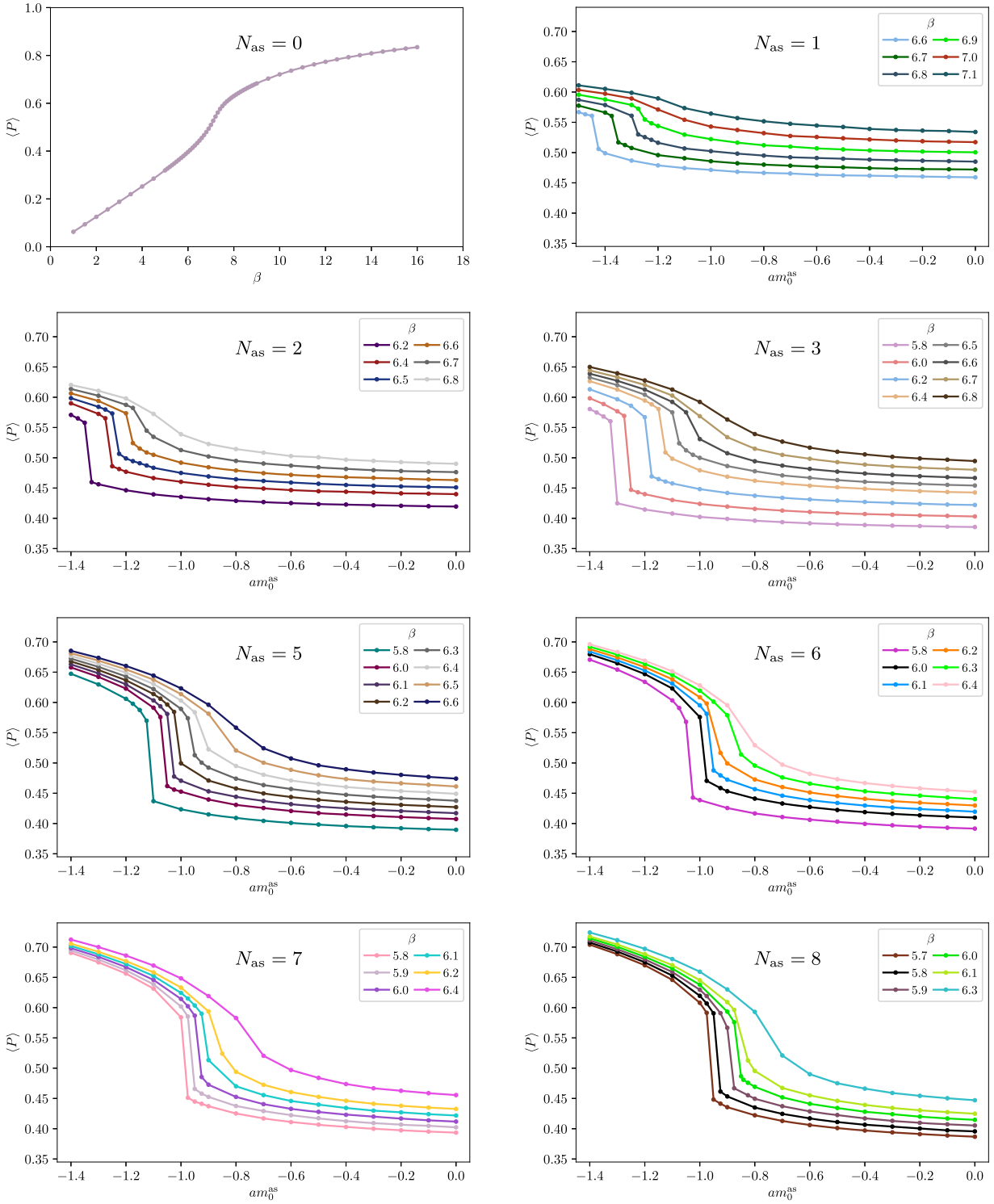

FIG. 14. Parameter scan in the $Sp(4)$ theory with $N_{\rm as} = 0, 1, 2, 3, 5, 6, 7, 8$ (left to right and top to bottom panels) fermions in the 2-index antisymmetric representation, obtained with ensembles generated from a cold start. For $N_{\rm as} > 0$, we show the value of the average plaquette, $\langle P \rangle$, as a function of the bare mass, for a few representative values of the coupling. For pure gauge, we just vary the value of β. All the fermions are treated with the HMC/RHMC algorithms. The lattice size is $\tilde{V} = (8a)^4$ and the base mass is chosen in the range $-1.4 \leq am_0^{\rm as} \leq 0.0$ for $N_{\rm as} \geq 2$, and $-1.5 \leq am_0^{\rm as} \leq 0.0$ for $N_{\rm as} = 1$. For the pure gauge theory, the coupling is chosen to be $1.0 \leq \beta \leq 16.0$. For $N_{\rm as} = 1$, we have chosen $\beta = 7.1, 7.0, 6.9, 6.8, 6.7, 6.6$, while for $N_{\rm as} = 2$ we have $\beta = 6.8, 6.7, 6.6, 6.5, 6.4, 6.2$. For $N_{\rm as} = 3$, the coupling is $\beta = 6.8, 6.7, 6.6, 6.5, 6.4, 6.2, 6.0, 5.8$, while for $N_{\rm as} = 5$ we have chosen $\beta = 6.6, 6.5, 6.4, 6.3, 6.2, 6.1, 6.0, 5.8$. For $N_{\rm as} = 6$, $\beta = 6.4, 6.3, 6.2, 6.1, 6.0, 5.8$. For $N_{\rm as} = 7$, $\beta = 6.4, 6.2, 6.1, 6.0, 5.9, 5.8$ and for $N_{\rm as} = 8$, $\beta = 6.3, 6.1, 6.0, 5.9, 5.8, 5.7$.

VI. SCALE SETTING AND TOPOLOGY

We return now to the theory with $N = 2$, $N_f = 0$, and $N_{as} = 4$. We discuss a scale setting procedure that uses the Wilson flow. We also monitor the evolution of the topological charge, to show that topological freezing was avoided. We focus the discussion on a few representative examples, although we checked that our conclusions have general validity for all choices of parameter relevant to this study.

The gradient flow [332], and its discretized counterpart, the Wilson flow [333], are useful for two complementary purposes. On the one hand, the Wilson flow provides a universal, well defined way to set the scale in a lattice theory, that is unambiguously defined irrespectively of the properties of the theory and of model-dependent considerations. On the other hand, the process we will describe momentarily consists of taking gauge configurations and evolving them with a flow equation, which results in the smoothing of such configurations, and the softening of short-distance fluctuations. The former property is beneficial because it allows to compare to one another different theories for which no experimental information is available (yet), and that might have different matter content. The latter characteristic allows, in practical terms, to reduce the short-distance numerical noise and the effects of discretization in the lattice calculation of observables, such as the topological charge, Q, which are sensitive to fluctuations at all scales.

We follow Refs. [1,11] (and references therein). One introduces the flow time, t, as an additional, fifth component of the space-time variables, and solves the defining differential equation

$$\frac{dB_\mu(x,t)}{dt} = D_\nu G_{\nu\mu}(x,t), \tag{36}$$

subject to the boundary conditions $B_\mu(x,0) = A_\mu(x)$. Here $A_\mu(x)$ are the gauge fields, and the covariant derivatives are $D_\mu \equiv \partial_\mu + [B_\mu, \cdot]$, and $G_{\mu\nu}(t) = [D_\mu, D_\nu]$. As anticipated, the main action of the flow is to introduce a Gaussian smoothing of the configurations, with mean-square radius $\sqrt{8t}$.

In order to use this object to introduce a scale, one defines the quantities

$$\mathcal{E}(t) \equiv \frac{t^2}{2}\langle \mathrm{Tr}[G_{\mu\nu}(t)G_{\mu\nu}(t)]\rangle, \tag{37}$$

$$\mathcal{W}(t) \equiv t\frac{d}{dt}\mathcal{E}(t), \tag{38}$$

and introduces a prescription that defines the scale on the basis of a reference value for either of the two. Two common choices in the literature are the scale, t_0, defined by setting

$$\mathcal{E}(t)|_{t=t_0} = \mathcal{E}_0, \tag{39}$$

or the scale, w_0, defined implicitly by the condition

$$\mathcal{W}(t)|_{t=w_0^2} = \mathcal{W}_0. \tag{40}$$

Both $\mathcal{E}_0$ and $\mathcal{W}_0$ are set on the basis of theoretical considerations. For example, Ref. [11] advocates to set $\mathcal{W}_0 = c_w C_2(F)$, where $C_2(F) = (1+2N)/4$ is the quadratic Casimir operator of the fundamental representation in $Sp(2N)$ theories, and one sets $c_w = 0.5$, though other choices are possible.

On the discretized lattice, one replaces the gauge field, $A_\mu(x)$, with the link variable, $U_\mu(x)$, and the flow equation is rewritten by replacing $B_\mu(x,t)$ with the new $V_\mu(x,t)$

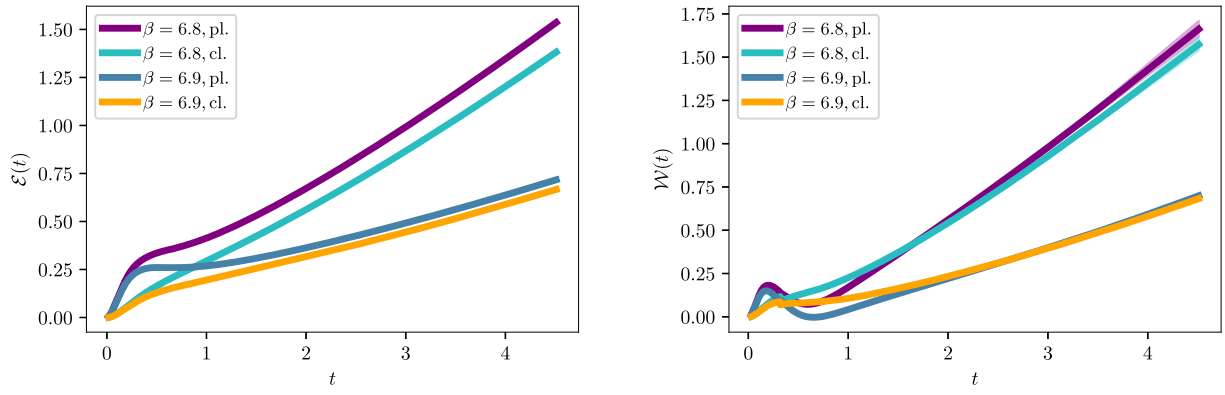

FIG. 15. Wilson Flow [332,333] energy density $\mathcal{E}(t)$ (left panel) and $\mathcal{W}(t)$ (right), computed as in Refs. [1,11], from the standard (pl) and the clover-leaf (cl) plaquette defined in Refs. [334,335], for the $Sp(4)$ theory with $N_{as} = 4$ fermions transforming in the 2-index antisymmetric representation. The lattice size is $\tilde{V} = (12a)^4$, and we display two representative choices of bare parameters, with $\beta = 6.8$ or 6.9 and common bare mass $am_0^{as} = -0.8$. The time step is 0.01, $t_{max} = 4.5$ to reduce finite-size effects. Errors are computed by bootstrapping. We have chosen $\mathcal{W}_0 = \frac{1}{2}C_2(F)$ for the topological charge. The corresponding values of w_0 from the plaquette and the clover-leaf are $w_{0,pl.} = 1.485(3)$ and $w_{0,cl.} = 1.495(2)$ for $\beta = 6.8$ and $w_{0,pl.} = 2.005(2)$ and $w_{0,cl.} = 2.026(2)$ for $\beta = 6.9$. We have set $a = 1$, for notational convenience.

[with $V_\mu(x,0) = U_\mu(x)$]. There are then at least two ways to replace $G_{\mu\nu}$ with a discretized variable. We introduced the elementary plaquette $\mathcal{P}_{\mu\nu}$ when defining the lattice action in Eq. (14). The clover-leaf plaquette operator, $\mathcal{C}_{\mu\nu}$, provides an alternative to the elementary plaquette, and can be seen as a simple form of improvement. We borrow the definition from Refs. [334,335], that for generic link variables $U_\mu(x)$ reads:

$$\begin{aligned}\mathcal{C}_{\mu\nu}(x) \equiv \frac{1}{8}\{&U_\mu(x)U_\nu(x+\hat{\mu})U_\mu^\dagger(x+\hat{\nu})U_\nu^\dagger(x)\\&+U_\nu(x)U_\mu^\dagger(x+\hat{\nu}-\hat{\mu})U_\nu^\dagger(x-\hat{\mu})U_\mu(x-\hat{\mu})\\&+U_\mu^\dagger(x-\hat{\mu})U_\nu^\dagger(x-\hat{\nu}-\hat{\mu})U_\mu(x-\hat{\nu}-\hat{\mu})U_\nu(x-\hat{\nu})\\&+U_\nu^\dagger(x-\hat{\nu})U_\mu(x-\hat{\nu})U_\nu(x-\hat{\nu}+\hat{\mu})U_\mu^\dagger(x)-\text{H.c.}\}.\end{aligned} \tag{41}$$

In principle, one would like to set the scale in a way that does not depend crucially on microscopic details. The scale setting using Wilson flow depends on the way the flow equation in Eq. (36) is latticized and how the observable $\mathrm{Tr}[G_{\mu\nu}G_{\mu\nu}]$ in Eq. (37) is discretized. Therefore, different choices lead to different values for the scale at a given cutoff, but choosing a suitable flow time t allows us to set the scale while reducing drastically these effects. To this purpose, in Fig. 15 we consider the $Sp(4)$ theory with $N_\mathrm{f} = 0$ and $N_\mathrm{as} = 4$, for two representative choices of β, and a representative choice of volume, $\tilde{V}$, and bare mass, am_0^as, and we show $\mathcal{E}(t)$ and $\mathcal{W}(t)$ as functions of the flow time, t, by comparing explicitly the results obtained by adopting either the elementary or the cloverleaf plaquette as defining the lattice regularization of the action. The plots illustrate the general trend evidenced elsewhere in the literature, according to which the function $\mathcal{W}(t)$ displays a milder dependence on the short distance regulator. In the following, we set the scale w_0 by conventionally setting $\mathcal{W}_0 = \frac{1}{2}C_2(F)$. Recently, several studies for the usage of the Wilson flow observables were performed to define a nonperturbative running coupling–see, e.g., Refs. [336–340] and [341] for a review. This is a very intriguing application of these tools, but it requires a dedicated study with non-negligible effort and large lattices, which exceed the lattice sizes we explored in this introductory paper.

The topological charge density is defined as

$$q_L(x,t) \equiv \frac{1}{32\pi^2}\varepsilon^{\mu\nu\rho\sigma}\mathrm{Tr}[\mathcal{C}_{\mu\nu}(x,t)\mathcal{C}_{\rho\sigma}(x,t)], \tag{42}$$

and the topological charge is $Q_L(t) \equiv \sum_x q_L(x,t)$, where, again, t is the flow time. In general, the topological charge on the lattice is not quantized, and in cases where it is the physical quantity of interest—for example because one is working toward a determination of the topological susceptibility, as in Ref. [11] and references therein—one needs to evolve to large t, and introduce a rounding process.

For the current purposes, we do not need a discretization algorithm: what we want to verify is that there is no evidence of topological freezing, and to this purpose we perform three simple tests. In Fig. 16 we display the value of $Q_L(t = w_0^2)$ in the $Sp(4)$ theory coupled to $N_\mathrm{f} = 0$ and $N_\mathrm{as} = 4$ fermion species, for two values of the coupling, β, and a common value of the bare mass. We show how the topological charge evolves along the trajectories, and supplement it with a histogram displaying its distribution. Both visual tests confirm that there is no evidence of topological freezing. We can make these tests more

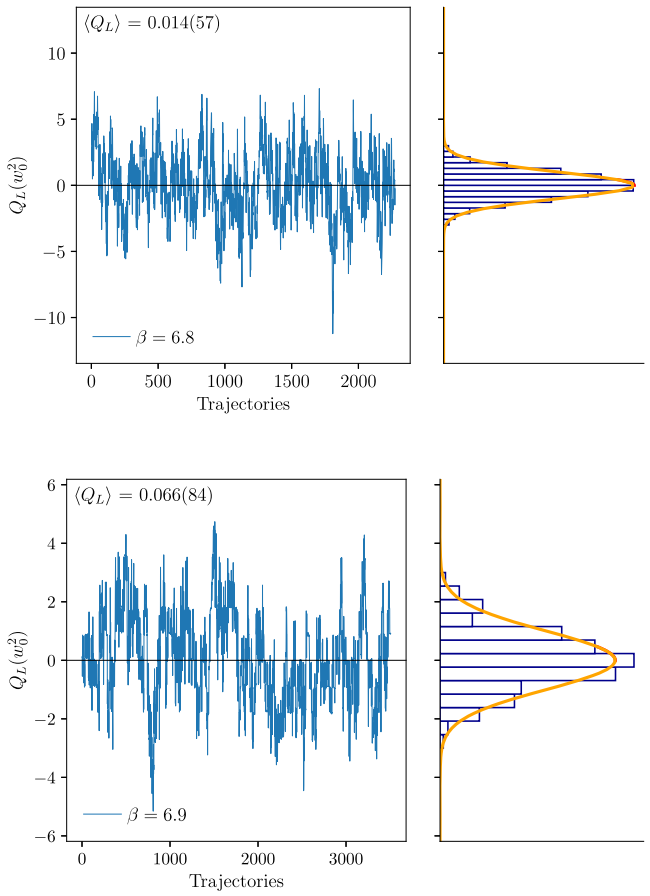

FIG. 16. Evolution with the ensemble trajectories of the topological charge $Q_L(t = w_0^2) \equiv \sum_x \frac{1}{32\pi^2}\varepsilon^{\mu\nu\rho\sigma}\mathrm{Tr}[\mathcal{C}_{\mu\nu}(x)\mathcal{C}_{\rho\sigma}(x)]$, computed (without rounding) at flow time $t = w_0^2$ for the $Sp(4)$ theory with $N_\mathrm{as} = 4$ fermions transforming in the 2-index antisymmetric representation. The lattice size is $\tilde{V} = (12a)^4$. The lattice parameters characterizing the ensembles are $\beta = 6.8$ (top panel) and $\beta = 6.9$ (bottom), with bare mass $am_0^\mathrm{as} = -0.8$. The histograms of the measurements (right panels) are compatible with a normal distribution centered at zero, with reduced chi-square $\chi^2/N_\mathrm{d.o.f} = \tilde{\chi}^2 = 1.1$ for both panels. The integrated autocorrelation time computed using the Madras-Sokal windowing algorithm is $\tau_Q = 7.11(64)$ (top) and $\tau_Q = 59.58(92)$ (bottom)$\tau_Q = 31(3)$ (top) and $\tau_Q = 238(12)$ (bottom).

quantitative by applying the standard Madras-Sokal windowing algorithm [322], and provide estimates of the integrated autocorrelation time τ_Q of the topological charge, which in both examples, as shown in Fig. 15, turns out to be many orders of magnitude smaller than the number of trajectories. Furthermore, fits of the histograms are compatible with a Gaussian distribution centered at $\langle Q_L(t = w_0^2)\rangle = 0$.

The main message from this section is that the behavior of the Wilson flow and of the topological charge, computed using the new software based on Grid, and tested on GPU architecture machines, to examine the properties of the lattice $Sp(2N)$ gauge theory with $N = 2$, $N_f = 0$, and $N_{as} = 4$, provide results that are broadly comparable to those in the literature for related, though different, field theories. This suggests that the implementation of the simulation routines and of the observables are both free from unwanted effects.

VII. SUMMARY AND OUTLOOK

A number of new physics models based upon $Sp(2N)$ gauge theories has been proposed in the literature, in such diverse contexts to include Composite Higgs Models, top partial compositeness, dilaton-Higgs models, strongly interacting dark matter models, among others. It is essential to the development of all these new physics ideas to provide model builders and phenomenologists with nontrivial information about the nonperturbative dynamics.

The programme of systematic characterization of $Sp(2N)$ theories is still in its early stages, though. Prominently, the challenging question of identifying the lower end of the conformal window in these theories coupled to matter fields in various representations of the group requires the nonperturbative instruments of lattice field theory. As a necessary step in this direction, we developed and tested new software, embedded into the Grid environment to take full advantage of its flexibility. In this paper we reported the (positive) results of our tests of the algorithms, that set the stage for future large-scale dedicated studies. We focused particularly on the $Sp(4)$ theory coupled to $N_{as} = 4$ (Dirac) fermions transforming in the antisymmetric representation, that might be close to the onset of conformality.

We performed a long list of non-trivial exercises. We both tested the effectiveness of the algorithm and software implementation, but also provided a first characterization of lattice theories that had never been studied before—although for present purposes we used comparatively small and coarse lattices. We reported in this paper illustrative examples demonstrating that there are no obvious problems in the software implementation. We computed effectively such observables as the averages of the plaquette and (real) Polyakov loop, the plaquette susceptibility, the Wilson flow, and the topological charge. We cataloged the first measurements of the critical couplings in $Sp(4)$ lattice theories with $N_{as} < 33/4$—below the bound imposed by asymptotic freedom—hence identifying the portion of lattice parameter space connected with the continuum theories of interest.

This paper, and the software we developed for it, set the stage needed to explore and quantify the extent of the conformal window in these theories. The tools we developed can be used also in the context of the recent literature discussing the spectroscopy of $Sp(2N)$ theories with various representations [1–19], in broad regions of their parameter space, considering both bosonic bound states as well as fermionic ones, relevant for example in $Sp(2N)$ theories with mixed representations. This effort can be complemented and further extended by applying new techniques based on the spectral densities [342]—see also the applications in Refs. [317,343–351]. One can envision many more uses and applications of this powerful and flexible open-source software.

Research Data Access Statement. The data generated for this manuscript can be downloaded from Ref. [352] and the analysis code from Ref. [353].

ACKNOWLEDGMENTS

The work of E. B., J. L., and B. L. has been funded by the Theoretical and Experimental Particle Physics at the Exascale Frontier (ExaTEPP) project No. EP/X017168/1. The work of E. B. and J. L. has also been supported by the UKRI Science and Technology Facilities Council (STFC) Research Software Engineering Fellowship EP/V052489/1. The work of N. F. has been supported by the STFC Consolidated Grant No. ST/X508834/1. The work of P. B. was supported in part by U.S. DOE Contract No. DESC0012704(BNL), and in part by the Scientific Discovery through Advanced Computing (SciDAC) program LAB 22-2580. The work of D. K. H. was supported by Basic Science Research Program through the National Research Foundation of Korea (NRF) funded by the Ministry of Education (NRF-2017R1D1A1B06033701). The work of L. D. D. and A. L. was supported by the ExaTEPP project EP/X01696X/1. The work of J. W. L. was supported in part by the National Research Foundation of Korea (NRF) grant funded by the Korea government(MSIT) (NRF-2018R1C1B3001379) and by IBS under the project code, IBS-R018-D1. The work of D. K. H. and J. W. L. was further supported by the National Research Foundation of Korea (NRF) grant funded by the Korea government (MSIT) (2021R1A4A5031460). The work of C. J. D. L. is supported by the Taiwanese NSTC Grant No. 109-2112-M-009-006-MY3. D. V. is supported by a STFC new applicant scheme grant. The work of B. L. and M. P. has been supported in part by the STFC Consolidated Grants No. ST/P00055X/1 and No. ST/T000813/1. B. L., M. P., A. L., and L. D. D. received funding from the European Research Council (ERC) under the European Union's Horizon 2020 research and innovation program

under Grant Agreement No. 813942. The work of B. L. is further supported in part by the EPSRC ExCALIBUR programme ExaTEPP (project EP/X017168/1), by the Royal Society Wolfson Research Merit Award WM170010 and by the Leverhulme Trust Research Fellowship No. RF-2020-4619. L. D. D. is supported by the UK Science and Technology Facility Council (STFC) grant No. ST/P000630/1. Numerical simulations have been performed on the Swansea SUNBIRD cluster (part of the Supercomputing Wales project) and AccelerateAI A100 GPU system, and on the DiRAC Extreme Scaling service at the University of Edinburgh. Supercomputing Wales and AccelerateAI are part funded by the European Regional Development Fund (ERDF) via Welsh Government. The DiRAC Extreme Scaling service is operated by the Edinburgh Parallel Computing Centre on behalf of the STFC DiRAC HPC Facility (www.dirac.ac.uk). This equipment was funded by BEIS capital funding via STFC capital Grant No. ST/R00238X/1 and STFC DiRAC Operations grant No. ST/R001006/1. DiRAC is part of the National e-Infrastructure.

APPENDIX A: GROUP-THEORETICAL DEFINITIONS

We denote as $Sp(2N)$ the subgroup of $SU(2N)$ preserving the norm induced by the antisymmetric matrix Ω,

$$\Omega = \begin{pmatrix} 0 & \mathbb{1}_N \\ -\mathbb{1}_N & 0 \end{pmatrix}, \tag{A1}$$

where $\mathbb{1}_N$ is the $N \times N$ identity matrix. This definition can be converted into a constraint on the group element U

$$U\Omega U^T = \Omega. \tag{A2}$$

Due to unitarity, the previous condition can be also written as

$$U\Omega = \Omega U^*, \tag{A3}$$

which implies the following block structure

$$U = \begin{pmatrix} A & B \\ -B^* & A^* \end{pmatrix}, \tag{A4}$$

where Eq. (A2) implies, for A and B, that

$$AB^T = BA^T, \qquad AA^\dagger + BB^\dagger = \mathbb{1}_N. \tag{A5}$$

The algebra can be defined by expanding $U\Omega = \Omega U^*$ in terms of the Hermitian generators t^a, i.e., $U = \exp(i\omega^a t^a)$ for real parameters ω^a. We arrive at the following condition on the generic element of the algebra $T = \sum_a \omega^a t^a$

$$T\Omega = -\Omega T^*, \tag{A6}$$

which also implies that

$$T = \begin{pmatrix} X & Y \\ Y^* & -X^* \end{pmatrix}. \tag{A7}$$

Hermiticity imposes the conditions $X = X^\dagger$ and $Y = Y^T$. The number of independent degrees of freedom is then $2N(N+1)$, the dimension of the group.

APPENDIX B: GENERATORS OF THE ALGEBRA IN GRID

Let t^a_{f} be the generators of the Lie algebra of $Sp(2N)$ in the fundamental representation. They are implemented in Grid as Hermitian, meaning that they follow the block structure of Eq. (A7). Their normalization is such that

$$\mathrm{Tr}(t^a_{\mathrm{f}} t^b_{\mathrm{f}}) = \frac{\delta^{ab}}{2}. \tag{B1}$$

The generators t^a_{f}, with $a = 1, \ldots, 2N^2 + N$, are implemented in Grid according to the following scheme. The $2N^2$ off-diagonal generators are identified by the following six relations among their matrix elements:

$$t^a_{i,j} = t^a_{j,i} = -t^a_{i+N,j+N} = -t^a_{j+N,i+N} = \frac{1}{2\sqrt{2}}, \quad i = 1, \ldots N-1, \quad i < j \le N, \tag{B2}$$

with $a = 1 \ldots N(N-1)/2$,

$$t^a_{i,j} = -t^a_{j,i} = t^a_{i+N,j+N} = -t^a_{j+N,i+N} = \frac{i}{2\sqrt{2}}, \quad i = 1, \ldots, N-1, \quad i < j \le N, \tag{B3}$$

with $a = N(N-1)/2 + 1 \ldots N(N-1)$,

$$t^a_{i,j+N} = t^a_{j,i+N} = t^a_{i+N,j} = t^a_{j+N,i} = \frac{1}{2\sqrt{2}}, \quad i = 1, \ldots, N-1, \quad i < j \le N-1, \tag{B4}$$

with $a = N(N-1) + 1 \ldots 3N(N-1)/2$,

$$t^a_{i,j+N} = t^a_{j,i+N} = -t^a_{i+N,j} = -t^a_{j+N,i} = \frac{i}{2\sqrt{2}}, \quad i = 1, \ldots, N-1, \qquad i < j \leq N-1, \tag{B5}$$

with $a = 3N(N-1)/2 + 1 \ldots 2N(N-1)$

$$t^a_{i,i+N} = t^a_{i+N,i} = \frac{1}{2}, \quad i = 1, \ldots, N, \tag{B6}$$

with $a = 2N^2 - 2N + 1 \ldots, 2N^2 - N$,

$$t^a_{i,i+N} = -t^a_{i+N,i} = \frac{i}{2}, \quad i = 1, \ldots, N, \tag{B7}$$

with $a = 2N^2 - N + 1, \ldots, 2N^2$. The remaining N generators in the Cartan subalgebra are

$$(t^a)_{i,i} = -(t^a)_{i+N,i+N} = \frac{1}{2}, \quad i = 1, \ldots N, \tag{B8}$$

with $a = 2N^2 + 1 \ldots 2N^2 + N$, the dimension of the group. It is useful to provide an explicit representation for $2N = 4$:

$$t^1_{\rm f} = \frac{1}{2\sqrt{2}}\begin{pmatrix} 0 & 1 & 0 & 0 \\ 1 & 0 & 0 & 0 \\ 0 & 0 & 0 & -1 \\ 0 & 0 & -1 & 0 \end{pmatrix} \quad t^6_{\rm f} = \frac{1}{2}\begin{pmatrix} 0 & 0 & 0 & 0 \\ 0 & 0 & 0 & 1 \\ 0 & 0 & 0 & 0 \\ 0 & 1 & 0 & 0 \end{pmatrix}$$

$$t^2_{\rm f} = \frac{1}{2\sqrt{2}}\begin{pmatrix} 0 & i & 0 & 0 \\ -i & 0 & 0 & 0 \\ 0 & 0 & 0 & i \\ 0 & 0 & -i & 0 \end{pmatrix} \quad t^7_{\rm f} = \frac{1}{2}\begin{pmatrix} 0 & 0 & i & 0 \\ 0 & 0 & 0 & 0 \\ -i & 0 & 0 & 0 \\ 0 & 0 & 0 & 0 \end{pmatrix}$$

$$t^3_{\rm f} = \frac{1}{2\sqrt{2}}\begin{pmatrix} 0 & 0 & 0 & 1 \\ 0 & 0 & 1 & 0 \\ 0 & 1 & 0 & 0 \\ 1 & 0 & 0 & 0 \end{pmatrix} \quad t^8_{\rm f} = \frac{1}{2}\begin{pmatrix} 0 & 0 & 0 & 0 \\ 0 & 0 & 0 & i \\ 0 & 0 & 0 & 0 \\ 0 & -i & 0 & 0 \end{pmatrix}$$

$$t^4_{\rm f} = \frac{1}{2\sqrt{2}}\begin{pmatrix} 0 & 0 & 0 & i \\ 0 & 0 & i & 0 \\ 0 & -i & 0 & 0 \\ -i & 0 & 0 & 0 \end{pmatrix} \quad t^9_{\rm f} = \frac{1}{2}\begin{pmatrix} 1 & 0 & 0 & 0 \\ 0 & 0 & 0 & 0 \\ 0 & 0 & -1 & 0 \\ 0 & 0 & 0 & 0 \end{pmatrix}$$

$$t^5_{\rm f} = \frac{1}{2}\begin{pmatrix} 0 & 0 & 1 & 0 \\ 0 & 0 & 0 & 0 \\ 1 & 0 & 0 & 0 \\ 0 & 0 & 0 & 0 \end{pmatrix} \quad t^{10}_{\rm f} = \frac{1}{2}\begin{pmatrix} 0 & 0 & 0 & 0 \\ 0 & 1 & 0 & 0 \\ 0 & 0 & 0 & 0 \\ 0 & 0 & 0 & -1 \end{pmatrix}. \tag{B9}$$

[1] E. Bennett, D. K. Hong, J. W. Lee, C.-J. D. Lin, B. Lucini, M. Piai, and D. Vadacchino, Sp(4) gauge theory on the lattice: Towards SU(4)/Sp(4) composite Higgs (and beyond), J. High Energy Phys. 03 (2018) 185.

[2] J. W. Lee, E. Bennett, D. K. Hong, C. J. D. Lin, B. Lucini, M. Piai, and D. Vadacchino, Progress in the lattice simulations of Sp($2N$) gauge theories, Proc. Sci. LATTICE2018 (**2018**) 192.

[3] E. Bennett, D. K. Hong, J. W. Lee, C. J. D. Lin, B. Lucini, M. Piai, and D. Vadacchino, Sp(4) gauge theories on the lattice: $N_f = 2$ dynamical fundamental fermions, J. High Energy Phys. 12 (2019) 053.

[4] E. Bennett, D. K. Hong, J. W. Lee, C. J. D. Lin, B. Lucini, M. Mesiti, M. Piai, J. Rantaharju, and D. Vadacchino, $Sp(4)$ gauge theories on the lattice: Quenched fundamental and antisymmetric fermions, Phys. Rev. D **101**, 074516 (2020).

[5] E. Bennett, J. Holligan, D. K. Hong, J. W. Lee, C. J. D. Lin, B. Lucini, M. Piai, and D. Vadacchino, Color dependence of tensor and scalar glueball masses in Yang-Mills theories, Phys. Rev. D **102**, 011501 (2020).

[6] E. Bennett, J. Holligan, D. K. Hong, J. W. Lee, C. J. D. Lin, B. Lucini, M. Piai, and D. Vadacchino, Glueballs and strings in $Sp(2N)$ Yang-Mills theories, Phys. Rev. D **103**, 054509 (2021).

[7] B. Lucini, E. Bennett, J. Holligan, D. K. Hong, H. Hsiao, J. W. Lee, C. J. D. Lin, M. Mesiti, M. Piai, and D. Vadacchino, Sp(4) gauge theories and beyond the standard model physics, EPJ Web Conf. **258**, 08003 (2022).

[8] E. Bennett, J. Holligan, D. K. Hong, H. Hsiao, J. W. Lee, C. J. D. Lin, B. Lucini, M. Mesiti, M. Piai, and D. Vadacchino, Progress in $Sp(2N)$ lattice gauge theories, Proc. Sci. LATTICE2021 (**2022**) 308.

[9] E. Bennett, D. K. Hong, H. Hsiao, J. W. Lee, C. J. D. Lin, B. Lucini, M. Mesiti, M. Piai, and D. Vadacchino, Lattice studies of the Sp(4) gauge theory with two fundamental

and three antisymmetric Dirac fermions, Phys. Rev. D **106**, 014501 (2022).
[10] E. Bennett, D. K. Hong, J. W. Lee, C. J. D. Lin, B. Lucini, M. Piai, and D. Vadacchino, Color dependence of the topological susceptibility in Yang-Mills theories, Phys. Lett. B **835**, 137504 (2022).
[11] E. Bennett, D. K. Hong, J. W. Lee, C. J. D. Lin, B. Lucini, M. Piai, and D. Vadacchino, Sp(2N) Yang-Mills theories on the lattice: Scale setting and topology, Phys. Rev. D **106**, 094503 (2022).
[12] E. Bennett, D. K. Hong, H. Hsiao, J. W. Lee, C. J. D. Lin, B. Lucini, M. Piai, and D. Vadacchino, Sp(4) theories on the lattice: Dynamical antisymmetric fermions (to be published).
[13] J. W. Lee, E. Bennett, D. K. Hong, H. Hsiao, C. J. D. Lin, B. Lucini, M. Piai, and D. Vadacchino, Spectroscopy of $Sp(4)$ lattice gauge theory with $n_f = 3$ antisymmetric fermions, Proc. Sci. LATTICE2022 (**2023**) 214.
[14] H. Hsiao, E. Bennett, D. K. Hong, J. W. Lee, C. J. D. Lin, B. Lucini, M. Piai, and D. Vadacchino, Spectroscopy of chimera baryons in a $Sp(4)$ lattice gauge theory, Proc. Sci. LATTICE2022 (**2023**) 211.
[15] E. Bennett, H. Hsiao, J. W. Lee, B. Lucini, A. Maas, M. Piai, and F. Zierler, Singlets in gauge theories with fundamental matter, arXiv:2304.07191.
[16] A. Maas and F. Zierler, Strong isospin breaking in Sp(4) gauge theory, Proc. Sci. LATTICE2021 (**2022**) 130.
[17] F. Zierler and A. Maas, $Sp(4)$ SIMP dark matter on the lattice, Proc. Sci. LHCP2021 (**2021**) 162.
[18] S. Kulkarni, A. Maas, S. Mee, M. Nikolic, J. Pradler, and F. Zierler, Low-energy effective description of dark Sp(4) theories, SciPost Phys. **14**, 044 (2023).
[19] E. Bennett, J. Holligan, D. K. Hong, H. Hsiao, J. W. Lee, C. J. D. Lin, B. Lucini, M. Mesiti, M. Piai, and D. Vadacchino, $Sp(2N)$ lattice gauge theories and extensions of the standard model of particle physics, Universe **9**, 236 (2023).
[20] J. Barnard, T. Gherghetta, and T. S. Ray, UV descriptions of composite Higgs models without elementary scalars, J. High Energy Phys. 02 (2014) 002.
[21] D. B. Kaplan and H. Georgi, $SU(2) \times U(1)$ breaking by vacuum misalignment, Phys. Lett. **136B**, 183 (1984).
[22] H. Georgi and D. B. Kaplan, Composite Higgs and Custodial SU(2), Phys. Lett. **145B**, 216 (1984).
[23] M. J. Dugan, H. Georgi, and D. B. Kaplan, Anatomy of a composite Higgs model, Nucl. Phys. **B254**, 299 (1985).
[24] G. Panico and A. Wulzer, The composite Nambu-Goldstone Higgs, Lect. Notes Phys. **913**, pp. 1 (2016).
[25] O. Witzel, Review on composite Higgs models, Proc. Sci. LATTICE2018 (**2019**) 006.
[26] G. Cacciapaglia, C. Pica, and F. Sannino, Fundamental composite dynamics: A review, Phys. Rep. **877**, 1 (2020).
[27] G. Ferretti and D. Karateev, Fermionic UV completions of composite Higgs models, J. High Energy Phys. 03 (2014) 077.
[28] G. Ferretti, Gauge theories of partial compositeness: Scenarios for run-II of the LHC, J. High Energy Phys. 06 (2016) 107.
[29] G. Cacciapaglia, G. Ferretti, T. Flacke, and H. Serôdio, Light scalars in composite Higgs models, Front. Phys. **7**, 22 (2019).
[30] E. Katz, A. E. Nelson, and D. G. E. Walker, The intermediate Higgs, J. High Energy Phys. 08 (2005) 074.
[31] R. Barbieri, B. Bellazzini, V. S. Rychkov, and A. Varagnolo, The Higgs boson from an extended symmetry, Phys. Rev. D **76**, 115008 (2007).
[32] P. Lodone, Vector-like quarks in a composite Higgs model, J. High Energy Phys. 12 (2008) 029.
[33] B. Gripaios, A. Pomarol, F. Riva, and J. Serra, Beyond the minimal composite Higgs model, J. High Energy Phys. 04 (2009) 070.
[34] J. Mrazek, A. Pomarol, R. Rattazzi, M. Redi, J. Serra, and A. Wulzer, The other natural two Higgs doublet model, Nucl. Phys. **B853**, 1 (2011).
[35] D. Marzocca, M. Serone, and J. Shu, General composite Higgs models, J. High Energy Phys. 08 (2012) 013.
[36] C. Grojean, O. Matsedonskyi, and G. Panico, Light top partners and precision physics, J. High Energy Phys. 10 (2013) 160.
[37] G. Cacciapaglia and F. Sannino, Fundamental composite (Goldstone) Higgs dynamics, J. High Energy Phys. 04 (2014) 111.
[38] G. Ferretti, UV completions of partial compositeness: The case for a SU(4) gauge group, J. High Energy Phys. 06 (2014) 142.
[39] A. Arbey, G. Cacciapaglia, H. Cai, A. Deandrea, S. Le Corre, and F. Sannino, Fundamental composite electroweak dynamics: Status at the LHC, Phys. Rev. D **95**, 015028 (2017).
[40] G. Cacciapaglia, H. Cai, A. Deandrea, T. Flacke, S. J. Lee, and A. Parolini, Composite scalars at the LHC: The Higgs, the sextet and the octet, J. High Energy Phys. 11 (2015) 201.
[41] F. Feruglio, B. Gavela, K. Kanshin, P. A. N. Machado, S. Rigolin, and S. Saa, The minimal linear sigma model for the Goldstone Higgs, J. High Energy Phys. 06 (2016) 038.
[42] T. DeGrand, M. Golterman, E. T. Neil, and Y. Shamir, One-loop chiral perturbation theory with two fermion representations, Phys. Rev. D **94**, 025020 (2016).
[43] S. Fichet, G. von Gersdorff, E. Pontòn, and R. Rosenfeld, The excitation of the global symmetry-breaking vacuum in composite Higgs models, J. High Energy Phys. 09 (2016) 158.
[44] J. Galloway, A. L. Kagan, and A. Martin, A UV complete partially composite-pNGB Higgs, Phys. Rev. D **95**, 035038 (2017).
[45] A. Agugliaro, O. Antipin, D. Becciolini, S. De Curtis, and M. Redi, UV complete composite Higgs models, Phys. Rev. D **95**, 035019 (2017).
[46] A. Belyaev, G. Cacciapaglia, H. Cai, G. Ferretti, T. Flacke, A. Parolini, and H. Serodio, Di-boson signatures as standard candles for partial compositeness, J. High Energy Phys. 01 (2017) 094.
[47] C. Csaki, T. Ma, and J. Shu, Maximally symmetric composite Higgs models, Phys. Rev. Lett. **119**, 131803 (2017).
[48] M. Chala, G. Durieux, C. Grojean, L. de Lima, and O. Matsedonskyi, Minimally extended SILH, J. High Energy Phys. 06 (2017) 088.

[49] M. Golterman and Y. Shamir, Effective potential in ultraviolet completions for composite Higgs models, Phys. Rev. D **97**, 095005 (2018).

[50] C. Csaki, T. Ma, and J. Shu, Trigonometric parity for composite Higgs models, Phys. Rev. Lett. **121**, 231801 (2018).

[51] T. Alanne, D. Buarque Franzosi, and M. T. Frandsen, A partially composite Goldstone Higgs, Phys. Rev. D **96**, 095012 (2017).

[52] T. Alanne, D. Buarque Franzosi, M. T. Frandsen, M. L. A. Kristensen, A. Meroni, and M. Rosenlyst, Partially composite Higgs models: Phenomenology and RG analysis, J. High Energy Phys. 01 (2018) 051.

[53] F. Sannino, P. Stangl, D. M. Straub, and A. E. Thomsen, Flavor physics and flavor anomalies in minimal fundamental partial compositeness, Phys. Rev. D **97**, 115046 (2018).

[54] T. Alanne, N. Bizot, G. Cacciapaglia, and F. Sannino, Classification of NLO operators for composite Higgs models, Phys. Rev. D **97**, 075028 (2018).

[55] N. Bizot, G. Cacciapaglia, and T. Flacke, Common exotic decays of top partners, J. High Energy Phys. 06 (2018) 065.

[56] C. Cai, G. Cacciapaglia, and H. H. Zhang, Vacuum alignment in a composite 2HDM, J. High Energy Phys. 01 (2019) 130.

[57] A. Agugliaro, G. Cacciapaglia, A. Deandrea, and S. De Curtis, Vacuum misalignment and pattern of scalar masses in the SU(5)/SO(5) composite Higgs model, J. High Energy Phys. 02 (2019) 089.

[58] G. Cacciapaglia, T. Ma, S. Vatani, and Y. Wu, Towards a fundamental safe theory of composite Higgs and dark matter, Eur. Phys. J. C **80**, 1088 (2020).

[59] H. Gertov, A. E. Nelson, A. Perko, and D. G. E. Walker, Lattice-friendly gauge completion of a composite Higgs with top partners, J. High Energy Phys. 02 (2019) 181.

[60] V. Ayyar, M. F. Golterman, D. C. Hackett, W. Jay, E. T. Neil, Y. Shamir, and B. Svetitsky, Radiative contribution to the composite-Higgs potential in a two-representation lattice model, Phys. Rev. D **99**, 094504 (2019).

[61] G. Cacciapaglia, H. Cai, A. Deandrea, and A. Kushwaha, Composite Higgs and dark matter model in SU(6)/SO(6), J. High Energy Phys. 10 (2019) 035.

[62] D. Buarque Franzosi and G. Ferretti, Anomalous dimensions of potential top-partners, SciPost Phys. **7**, 027 (2019).

[63] G. Cacciapaglia, S. Vatani, and C. Zhang, Composite Higgs meets Planck scale: Partial compositeness from partial unification, Phys. Lett. B **815**, 136177 (2021).

[64] G. Cacciapaglia, A. Deandrea, T. Flacke, and A. M. Iyer, Gluon-photon signatures for color octet at the LHC (and beyond), J. High Energy Phys. 05 (2020) 027.

[65] Z. Y. Dong, C. S. Guan, T. Ma, J. Shu, and X. Xue, UV completed composite Higgs model with heavy composite partners, Phys. Rev. D **104**, 035013 (2021).

[66] G. Cacciapaglia, T. Flacke, M. Kunkel, and W. Porod, Phenomenology of unusual top partners in composite Higgs models, J. High Energy Phys. 02 (2022) 208.

[67] A. Banerjee, D. B. Franzosi, and G. Ferretti, Modelling vector-like quarks in partial compositeness framework, J. High Energy Phys. 03 (2022) 200.

[68] G. Ferretti, Compositeness above the electroweak scale and a proposed test at LHCb, EPJ Web Conf. **258**, 08002 (2022).

[69] R. Contino, Y. Nomura, and A. Pomarol, Higgs as a holographic pseudoGoldstone boson, Nucl. Phys. **B671**, 148 (2003).

[70] K. Agashe, R. Contino, and A. Pomarol, The minimal composite Higgs model, Nucl. Phys. **B719**, 165 (2005).

[71] K. Agashe and R. Contino, The minimal composite Higgs model and electroweak precision tests, Nucl. Phys. **B742**, 59 (2006).

[72] K. Agashe, R. Contino, L. Da Rold, and A. Pomarol, A Custodial symmetry for $Zb\bar{b}$, Phys. Lett. B **641**, 62 (2006).

[73] R. Contino, L. Da Rold, and A. Pomarol, Light custodians in natural composite Higgs models, Phys. Rev. D **75**, 055014 (2007).

[74] A. Falkowski and M. Perez-Victoria, Electroweak breaking on a soft wall, J. High Energy Phys. 12 (2008) 107.

[75] R. Contino, The Higgs as a composite Nambu-Goldstone boson, in *Physics of the Large and the Small* (World Scientific, Singapore, 2011).

[76] R. Contino, D. Marzocca, D. Pappadopulo, and R. Rattazzi, On the effect of resonances in composite Higgs phenomenology, J. High Energy Phys. 10 (2011) 081.

[77] F. Caracciolo, A. Parolini, and M. Serone, UV completions of composite Higgs models with partial compositeness, J. High Energy Phys. 02 (2013) 066.

[78] J. Erdmenger, N. Evans, W. Porod, and K. S. Rigatos, Gauge/gravity dynamics for composite Higgs models and the top mass, Phys. Rev. Lett. **126**, 071602 (2021).

[79] J. Erdmenger, N. Evans, W. Porod, and K. S. Rigatos, Gauge/gravity dual dynamics for the strongly coupled sector of composite Higgs models, J. High Energy Phys. 02 (2021) 058.

[80] D. Elander, M. Frigerio, M. Knecht, and J. L. Kneur, Holographic models of composite Higgs in the Veneziano limit. Part I. Bosonic sector, J. High Energy Phys. 03 (2021) 182.

[81] D. Elander, M. Frigerio, M. Knecht, and J. L. Kneur, Holographic models of composite Higgs in the Veneziano limit. Part II. Fermionic sector, J. High Energy Phys. 05 (2022) 066.

[82] D. Elander and M. Piai, Towards top-down holographic composite Higgs: Minimal coset from maximal supergravity, J. High Energy Phys. 03 (2022) 049.

[83] D. Elander, A. Fatemiabhari, and M. Piai, Towards composite Higgs: Minimal coset from a regular bottom-up holographic model, Phys. Rev. D **107**, 115021 (2023).

[84] J. Erdmenger, N. Evans, Y. Liu, and W. Porod, Holographic non-Abelian flavour symmetry breaking, Universe **9**, 289 (2023).

[85] D. B. Kaplan, Flavor at SSC energies: A new mechanism for dynamically generated fermion masses, Nucl. Phys. **B365**, 259 (1991).

[86] Y. Grossman and M. Neubert, Neutrino masses and mixings in nonfactorizable geometry, Phys. Lett. B **474**, 361 (2000).

[87] T. Gherghetta and A. Pomarol, Bulk fields and supersymmetry in a slice of AdS, Nucl. Phys. **B586**, 141 (2000).

[88] Y. Hochberg, E. Kuflik, T. Volansky, and J. G. Wacker, Mechanism for thermal relic dark matter of strongly interacting massive particles, Phys. Rev. Lett. **113**, 171301 (2014).

[89] Y. Hochberg, E. Kuflik, H. Murayama, T. Volansky, and J. G. Wacker, Model for thermal relic dark matter of strongly interacting massive particles, Phys. Rev. Lett. **115**, 021301 (2015).

[90] Y. Hochberg, E. Kuflik, and H. Murayama, SIMP spectroscopy, J. High Energy Phys. 05 (2016) 090.

[91] A. Berlin, N. Blinov, S. Gori, P. Schuster, and N. Toro, Cosmology and accelerator tests of strongly interacting dark matter, Phys. Rev. D **97**, 055033 (2018).

[92] N. Bernal, X. Chu, and J. Pradler, Simply split strongly interacting massive particles, Phys. Rev. D **95**, 115023 (2017).

[93] N. Bernal, X. Chu, S. Kulkarni, and J. Pradler, Self-interacting dark matter without prejudice, Phys. Rev. D **101**, 055044 (2020).

[94] Y. D. Tsai, R. McGehee, and H. Murayama, Resonant self-interacting dark matter from dark QCD, Phys. Rev. Lett. **128**, 172001 (2022).

[95] D. Kondo, R. McGehee, T. Melia, and H. Murayama, Linear sigma dark matter, J. High Energy Phys. 09 (2022) 041.

[96] N. Bernal and X. Chu, $\mathbb{Z}_2$ SIMP dark matter, J. Cosmol. Astropart. Phys. 01 (2016) 006.

[97] W. J. G. de Blok, The core-cusp problem, Adv. Astron. **2010**, 789293 (2010).

[98] M. Boylan-Kolchin, J. S. Bullock, and M. Kaplinghat, Too big to fail? The puzzling darkness of massive milky way subhaloes, Mon. Not. R. Astron. Soc. **415**, L40 (2011).

[99] N. Seto, S. Kawamura, and T. Nakamura, Possibility of direct measurement of the acceleration of the universe using 0.1-Hz band laser interferometer gravitational wave antenna in space, Phys. Rev. Lett. **87**, 221103 (2001).

[100] S. Kawamura, T. Nakamura, M. Ando, N. Seto, K. Tsubono, K. Numata, R. Takahashi, S. Nagano, T. Ishikawa, M. Musha *et al.*, The Japanese space gravitational wave antenna DECIGO, Classical Quantum Gravity **23**, S125 (2006).

[101] J. Crowder and N. J. Cornish, Beyond LISA: Exploring future gravitational wave missions, Phys. Rev. D **72**, 083005 (2005).

[102] V. Corbin and N. J. Cornish, Detecting the cosmic gravitational wave background with the big bang observer, Classical Quantum Gravity **23**, 2435 (2006).

[103] G. M. Harry, P. Fritschel, D. A. Shaddock, W. Folkner, and E. S. Phinney, Laser interferometry for the big bang observer, Classical Quantum Gravity **23**, 4887 (2006); **23**, 7361(E) (2006).

[104] S. Hild, M. Abernathy, F. Acernese, P. Amaro-Seoane, N. Andersson, K. Arun, F. Barone, B. Barr, M. Barsuglia, M. Beker *et al.*, Sensitivity studies for third-generation gravitational wave observatories, Classical Quantum Gravity **28**, 094013 (2011).

[105] K. Yagi and N. Seto, Detector configuration of DECIGO/BBO and identification of cosmological neutron-star binaries, Phys. Rev. D **83**, 044011 (2011); **95**, 109901(E) (2017).

[106] B. Sathyaprakash, M. Abernathy, F. Acernese, P. Ajith, B. Allen, P. Amaro-Seoane, N. Andersson, S. Aoudia, K. Arun, P. Astone *et al.*, Scientific objectives of Einstein telescope, Classical Quantum Gravity **29**, 124013 (2012); **30**, 079501(E) (2013).

[107] E. Thrane and J. D. Romano, Sensitivity curves for searches for gravitational-wave backgrounds, Phys. Rev. D **88**, 124032 (2013).

[108] C. Caprini, M. Hindmarsh, S. Huber, T. Konstandin, J. Kozaczuk, G. Nardini, J. M. No, A. Petiteau, P. Schwaller, G. Servant *et al.*, Science with the space-based interferometer eLISA. II: Gravitational waves from cosmological phase transitions, J. Cosmol. Astropart. Phys. 04 (2016) 001.

[109] P. Amaro-Seoane *et al.* (LISA Collaboration), Laser interferometer space antenna, arXiv:1702.00786.

[110] B. P. Abbott *et al.* (LIGO Scientific Collaboration), Exploring the sensitivity of next generation gravitational wave detectors, Classical Quantum Gravity **34**, 044001 (2017).

[111] S. Isoyama, H. Nakano, and T. Nakamura, Multiband gravitational-wave astronomy: Observing binary inspirals with a decihertz detector, B-DECIGO, Prog. Theor. Exp. Phys. **2018**, 073E01 (2018).

[112] J. Baker, J. Bellovary, P. L. Bender, E. Berti, R. Caldwell, J. Camp, J. W. Conklin, N. Cornish, C. Cutler, R. DeRosa *et al.*, The laser interferometer space antenna: Unveiling the millihertz gravitational wave sky, arXiv:1907.06482.

[113] V. Brdar, A. J. Helmboldt, and J. Kubo, Gravitational waves from first-order phase transitions: LIGO as a window to unexplored Seesaw scales, J. Cosmol. Astropart. Phys. 02 (2019) 021.

[114] D. Reitze, R. X. Adhikari, S. Ballmer, B. Barish, L. Barsotti, G. Billingsley, D. A. Brown, Y. Chen, D. Coyne, R. Eisenstein *et al.*, Cosmic Explorer: The U.S. Contribution to gravitational-wave astronomy beyond LIGO, Bull. Am. Astron. Soc. **51**, 035 (2019).

[115] C. Caprini, M. Chala, G. C. Dorsch, M. Hindmarsh, S. J. Huber, T. Konstandin, J. Kozaczuk, G. Nardini, J. M. No, K. Rummukainen *et al.*, Detecting gravitational waves from cosmological phase transitions with LISA: An update, J. Cosmol. Astropart. Phys. 03 (2020) 024.

[116] M. Maggiore, C. Van Den Broeck, N. Bartolo, E. Belgacem, D. Bertacca, M. A. Bizouard, M. Branchesi, S. Clesse, S. Foffa, J. García-Bellido *et al.*, Science case for the Einstein telescope, J. Cosmol. Astropart. Phys. 03 (2020) 050.

[117] E. Witten, Cosmic separation of phases, Phys. Rev. D **30**, 272 (1984).

[118] M. Kamionkowski, A. Kosowsky, and M. S. Turner, Gravitational radiation from first order phase transitions, Phys. Rev. D **49**, 2837 (1994).

[119] B. Allen, The stochastic gravity wave background: Sources and detection, arXiv:gr-qc/9604033.

[120] P. Schwaller, Gravitational waves from a dark phase transition, Phys. Rev. Lett. **115**, 181101 (2015).

[121] D. Croon, V. Sanz, and G. White, Model discrimination in gravitational wave spectra from dark phase transitions, J. High Energy Phys. 08 (2018) 203.

[122] N. Christensen, Stochastic gravitational wave backgrounds, Rep. Prog. Phys. **82**, 016903 (2019).

[123] W. C. Huang, M. Reichert, F. Sannino, and Z. W. Wang, Testing the dark SU(N) Yang-Mills theory confined

landscape: From the lattice to gravitational waves, Phys. Rev. D **104**, 035005 (2021).
[124] J. Halverson, C. Long, A. Maiti, B. Nelson, and G. Salinas, Gravitational waves from dark Yang-Mills sectors, J. High Energy Phys. 05 (2021) 154.
[125] Z. Kang, J. Zhu, and S. Matsuzaki, Dark confinement-deconfinement phase transition: A roadmap from Polyakov loop models to gravitational waves, J. High Energy Phys. 09 (2021) 060.
[126] B. Lucini and M. Teper, SU(N) gauge theories in four-dimensions: Exploring the approach to N = infinity, J. High Energy Phys. 06 (2001) 050.
[127] B. Lucini, M. Teper, and U. Wenger, Glueballs and k-strings in SU(N) gauge theories: Calculations with improved operators, J. High Energy Phys. 06 (2004) 012.
[128] B. Lucini, A. Rago, and E. Rinaldi, Glueball masses in the large N limit, J. High Energy Phys. 08 (2010) 119.
[129] B. Lucini and M. Panero, SU(N) gauge theories at large N, Phys. Rep. **526**, 93 (2013).
[130] A. Athenodorou, R. Lau, and M. Teper, On the weak N -dependence of SO(N) and SU(N) gauge theories in $2+1$ dimensions, Phys. Lett. B **749**, 448 (2015).
[131] R. Lau and M. Teper, SO(N) gauge theories in $2+1$ dimensions: Glueball spectra and confinement, J. High Energy Phys. 10 (2017) 022.
[132] P. Hernández and F. Romero-López, The large N_c limit of QCD on the lattice, Eur. Phys. J. A **57**, 52 (2021).
[133] A. Athenodorou and M. Teper, SU(N) gauge theories in $3+1$ dimensions: Glueball spectrum, string tensions and topology, J. High Energy Phys. 12 (2021) 082.
[134] N. Yamanaka, A. Nakamura, and M. Wakayama, Inter-glueball potential in lattice SU(N) gauge theories, Proc. Sci. LATTICE2021 (**2022**) 447.
[135] C. Bonanno, M. D'Elia, B. Lucini, and D. Vadacchino, Towards glueball masses of large-N SU(N) pure-gauge theories without topological freezing, Phys. Lett. B **833**, 137281 (2022).
[136] M. Luscher, Topology of lattice gauge fields, Commun. Math. Phys. **85**, 39 (1982).
[137] M. Campostrini, A. Di Giacomo, H. Panagopoulos, and E. Vicari, Topological charge, renormalization and cooling on the lattice, Nucl. Phys. **B329**, 683 (1990).
[138] L. Del Debbio, H. Panagopoulos, and E. Vicari, theta dependence of SU(N) gauge theories, J. High Energy Phys. 08 (2002) 044.
[139] B. Lucini, M. Teper, and U. Wenger, Topology of SU(N) gauge theories at $T = {}^{\sim}0$ and $T = {}^{\sim}T(c)$, Nucl. Phys. **B715**, 461 (2005).
[140] L. Del Debbio, L. Giusti, and C. Pica, Topological susceptibility in the SU(3) gauge theory, Phys. Rev. Lett. **94**, 032003 (2005).
[141] M. Luscher and F. Palombi, Universality of the topological susceptibility in the SU(3) gauge theory, J. High Energy Phys. 09 (2010) 110.
[142] H. Panagopoulos and E. Vicari, The 4D SU(3) gauge theory with an imaginary θ term, J. High Energy Phys. 11 (2011) 119.
[143] C. Bonati, M. D'Elia, and A. Scapellato, θ dependence in $SU(3)$ Yang-Mills theory from analytic continuation, Phys. Rev. D **93**, 025028 (2016).
[144] C. Bonati, M. D'Elia, P. Rossi, and E. Vicari, θ dependence of 4D $SU(N)$ gauge theories in the large-N limit, Phys. Rev. D **94**, 085017 (2016).
[145] M. Cè, M. García Vera, L. Giusti, and S. Schaefer, The topological susceptibility in the large-N limit of SU(N) Yang–Mills theory, Phys. Lett. B **762**, 232 (2016).
[146] C. Alexandrou, A. Athenodorou, K. Cichy, A. Dromard, E. Garcia-Ramos, K. Jansen, U. Wenger, and F. Zimmermann, Comparison of topological charge definitions in Lattice QCD, Eur. Phys. J. C **80**, 424 (2020).
[147] C. Bonanno, C. Bonati, and M. D'Elia, Large-N $SU(N)$ Yang-Mills theories with milder topological freezing, J. High Energy Phys. 03 (2021) 111.
[148] S. Borsanyi and D. Sexty, Topological susceptibility of pure gauge theory using density of states, Phys. Lett. B **815**, 136148 (2021).
[149] G. Cossu, D. Lancastera, B. Lucini, R. Pellegrini, and A. Rago, Ergodic sampling of the topological charge using the density of states, Eur. Phys. J. C **81**, 375 (2021).
[150] M. Teper, More methods for calculating the topological charge (density) of SU(N) lattice gauge fields in $3+1$ dimensions, arXiv:2202.02528.
[151] C. Bonanno, M. D'Elia, B. Lucini, and D. Vadacchino, Towards glueball masses of large-N SU(N) Yang-Mills theories without topological freezing via parallel tempering on boundary conditions, Proc. Sci. LATTICE2022 (**2023**) 392.
[152] C. Bonanno, Lattice determination of the topological susceptibility slope χ' of 2d CPN-1 models at large N, Phys. Rev. D **107**, 014514 (2023).
[153] M. Bochicchio, An asymptotic solution of Large-N QCD, for the glueball and meson spectrum and the collinear S-matrix, AIP Conf. Proc. **1735**, 030004 (2016).
[154] M. Bochicchio, Glueball and meson spectrum in large-N massless QCD, arXiv:1308.2925.
[155] D. K. Hong, J. W. Lee, B. Lucini, M. Piai, and D. Vadacchino, Casimir scaling and Yang–Mills glueballs, Phys. Lett. B **775**, 89 (2017).
[156] K. Holland, M. Pepe, and U. J. Wiese, The deconfinement phase transition of Sp(2) and Sp(3) Yang-Mills theories in $(2+1)$-dimensions and $(3+1)$-dimensions, Nucl. Phys. **B694**, 35 (2004).
[157] W. E. Caswell, Asymptotic behavior of non-Abelian gauge theories to two loop order, Phys. Rev. Lett. **33**, 244 (1974).
[158] T. Banks and A. Zaks, On the phase structure of vector-like gauge theories with massless fermions, Nucl. Phys. **B196**, 189 (1982).
[159] K. A. Intriligator and N. Seiberg, Lectures on supersymmetric gauge theories and electric-magnetic duality, Nucl. Phys. B, Proc. Suppl. **45BC**, 1 (1996).
[160] T. Appelquist, K. D. Lane, and U. Mahanta, On the ladder approximation for spontaneous chiral symmetry breaking, Phys. Rev. Lett. **61**, 1553 (1988).
[161] A. G. Cohen and H. Georgi, Walking beyond the rainbow, Nucl. Phys. **B314**, 7 (1989).
[162] F. Sannino and K. Tuominen, Orientifold theory dynamics and symmetry breaking, Phys. Rev. D **71**, 051901 (2005).
[163] D. D. Dietrich and F. Sannino, Conformal window of SU(N) gauge theories with fermions in higher dimensional representations, Phys. Rev. D **75**, 085018 (2007).

[164] T. A. Ryttov and F. Sannino, Supersymmetry inspired QCD beta function, Phys. Rev. D **78**, 065001 (2008).

[165] C. Pica and F. Sannino, Beta function and anomalous dimensions, Phys. Rev. D **83**, 116001 (2011).

[166] C. Pica and F. Sannino, UV and IR zeros of gauge theories at the four loop order and beyond, Phys. Rev. D **83**, 035013 (2011).

[167] B. S. Kim, D. K. Hong, and J. W. Lee, Into the conformal window: Multirepresentation gauge theories, Phys. Rev. D **101**, 056008 (2020).

[168] J. W. Lee, Conformal window from conformal expansion, Phys. Rev. D **103**, 076006 (2021).

[169] P. A. Baikov, K. G. Chetyrkin, and J. H. Kühn, Five-loop running of the QCD coupling constant, Phys. Rev. Lett. **118**, 082002 (2017).

[170] F. Herzog, B. Ruijl, T. Ueda, J. A. M. Vermaseren, and A. Vogt, The five-loop beta function of Yang-Mills theory with fermions, J. High Energy Phys. 02 (2017) 090.

[171] T. A. Ryttov and R. Shrock, Infrared zero of β and Value of γ_m for an SU(3) gauge theory at the five-loop level, Phys. Rev. D **94**, 105015 (2016).

[172] T. A. Ryttov, Consistent perturbative fixed point calculations in QCD and supersymmetric QCD, Phys. Rev. Lett. **117**, 071601 (2016).

[173] T. A. Ryttov and R. Shrock, Scheme-independent calculation of $\gamma_{\bar{\psi}\psi,\mathrm{IR}}$ for an SU(3) gauge theory, Phys. Rev. D **94**, 105014 (2016).

[174] T. A. Ryttov and R. Shrock, Scheme-independent series expansions at an infrared zero of the beta function in asymptotically free gauge theories, Phys. Rev. D **94**, 125005 (2016).

[175] T. A. Ryttov and R. Shrock, Higher-order scheme-independent calculations of physical quantities in the conformal phase of a gauge theory, Phys. Rev. D **95**, 085012 (2017).

[176] T. A. Ryttov and R. Shrock, Higher-order scheme-independent series expansions of $\gamma_{\bar{\psi}\psi,\mathrm{IR}}$ and β'_{IR} in conformal field theories, Phys. Rev. D **95**, 105004 (2017).

[177] T. A. Ryttov and R. Shrock, Infrared fixed point physics in $\mathrm{SO}(N_c)$ and $\mathrm{Sp}(N_c)$ gauge theories, Phys. Rev. D **96**, 105015 (2017).

[178] J. A. Gracey, T. A. Ryttov, and R. Shrock, Scheme-independent calculations of anomalous dimensions of baryon operators in conformal field theories, Phys. Rev. D **97**, 116018 (2018).

[179] T. A. Ryttov and R. Shrock, Scheme-independent calculations of properties at a conformal infrared fixed point in gauge theories with multiple fermion representations, Phys. Rev. D **98**, 096003 (2018).

[180] T. A. Ryttov and R. Shrock, Scheme-independent series for anomalous dimensions of higher-spin operators at an infrared fixed point in a gauge theory, Phys. Rev. D **101**, 076018 (2020).

[181] T. A. Ryttov and R. Shrock, Anomalous dimensions at an infrared fixed point in an SU(Nc) gauge theory with fermions in the fundamental and antisymmetric tensor representations, Phys. Rev. D **108**, 056007 (2023).

[182] D. B. Kaplan, J. W. Lee, D. T. Son, and M. A. Stephanov, Conformality lost, Phys. Rev. D **80**, 125005 (2009).

[183] R. S. Chivukula, Lectures on technicolor and compositeness, arXiv:hep-ph/0011264.

[184] K. Lane, Two lectures on technicolor, arXiv:hep-ph/0202255.

[185] C. T. Hill and E. H. Simmons, Strong dynamics and electroweak symmetry breaking, Phys. Rep. **381**, 235 (2003); **390**, 553(E) (2004).

[186] A. Martin, Predicted signals at the LHC from technicolor: Erice lecture, Subnuclear series **46**, 135 (2011).

[187] F. Sannino, Conformal dynamics for TeV physics and cosmology, Acta Phys. Pol. B **40**, 3533 (2009).

[188] M. Piai, Lectures on walking technicolor, holography and gauge/gravity dualities, Adv. High Energy Phys. **2010**, 464302 (2010).

[189] K. Rummukainen and K. Tuominen, Lattice computations for beyond standard model physics, Universe **8**, 188 (2022).

[190] S. Catterall and F. Sannino, Minimal walking on the lattice, Phys. Rev. D **76**, 034504 (2007).

[191] L. Del Debbio, A. Patella, and C. Pica, Higher representations on the lattice: Numerical simulations. SU(2) with adjoint fermions, Phys. Rev. D **81**, 094503 (2010).

[192] A. J. Hietanen, J. Rantaharju, K. Rummukainen, and K. Tuominen, Spectrum of SU(2) lattice gauge theory with two adjoint Dirac flavours, J. High Energy Phys. 05 (2009) 025.

[193] T. Appelquist, G. T. Fleming, and E. T. Neil, Lattice study of conformal behavior in SU(3) Yang-Mills theories, Phys. Rev. D **79**, 076010 (2009).

[194] A. J. Hietanen, K. Rummukainen, and K. Tuominen, Evolution of the coupling constant in SU(2) lattice gauge theory with two adjoint fermions, Phys. Rev. D **80**, 094504 (2009).

[195] L. Del Debbio, B. Lucini, A. Patella, C. Pica, and A. Rago, Conformal versus confining scenario in SU(2) with adjoint fermions, Phys. Rev. D **80**, 074507 (2009).

[196] T. Appelquist *et al.* (LSD Collaboration), Toward TeV conformality, Phys. Rev. Lett. **104**, 071601 (2010).

[197] F. Bursa, L. Del Debbio, L. Keegan, C. Pica, and T. Pickup, Mass anomalous dimension in SU(2) with two adjoint fermions, Phys. Rev. D **81**, 014505 (2010).

[198] Z. Fodor, K. Holland, J. Kuti, D. Nogradi, and C. Schroeder, Chiral symmetry breaking in nearly conformal gauge theories, Proc. Sci. LAT2009 (**2009**) 055.

[199] L. Del Debbio, B. Lucini, A. Patella, C. Pica, and A. Rago, The infrared dynamics of minimal walking technicolor, Phys. Rev. D **82**, 014510 (2010).

[200] T. DeGrand, Y. Shamir, and B. Svetitsky, Running coupling and mass anomalous dimension of SU(3) gauge theory with two flavors of symmetric-representation fermions, Phys. Rev. D **82**, 054503 (2010).

[201] A. Patella, L. Del Debbio, B. Lucini, C. Pica, and A. Rago, Confining vs. conformal scenario for SU(2) with adjoint fermions. Gluonic observables, Proc. Sci. LATTICE2010 (**2010**) 068.

[202] M. Hayakawa, K. I. Ishikawa, Y. Osaki, S. Takeda, S. Uno, and N. Yamada, Running coupling constant of ten-flavor QCD with the Schrödinger functional method, Phys. Rev. D **83**, 074509 (2011).

[203] Z. Fodor, K. Holland, J. Kuti, D. Nogradi, C. Schroeder, K. Holland, J. Kuti, D. Nogradi, and C. Schroeder, Twelve

massless flavors and three colors below the conformal window, Phys. Lett. B **703**, 348 (2011).
[204] F. Bursa, L. Del Debbio, D. Henty, E. Kerrane, B. Lucini, A. Patella, C. Pica, T. Pickup, and A. Rago, Improved lattice spectroscopy of minimal walking technicolor, Phys. Rev. D **84**, 034506 (2011).
[205] T. Appelquist, G. T. Fleming, M. F. Lin, E. T. Neil, and D. A. Schaich, Lattice simulations and infrared conformality, Phys. Rev. D **84**, 054501 (2011).
[206] T. DeGrand, Finite-size scaling tests for spectra in SU(3) lattice gauge theory coupled to 12 fundamental flavor fermions, Phys. Rev. D **84**, 116901 (2011).
[207] T. Karavirta, J. Rantaharju, K. Rummukainen, and K. Tuominen, Determining the conformal window: SU(2) gauge theory with $N_f = 4$, 6 and 10 fermion flavours, J. High Energy Phys. 05 (2012) 003.
[208] T. DeGrand, Y. Shamir, and B. Svetitsky, SU(4) lattice gauge theory with decuplet fermions: Schrödinger functional analysis, Phys. Rev. D **85**, 074506 (2012).
[209] T. Appelquist, R. C. Brower, M. I. Buchoff, M. Cheng, S. D. Cohen, G. T. Fleming, J. Kiskis, M. Lin, H. Na, E. T. Neil *et al.*, Approaching conformality with ten flavors, arXiv:1204.6000.
[210] C. J. D. Lin, K. Ogawa, H. Ohki, and E. Shintani, Lattice study of infrared behaviour in SU(3) gauge theory with twelve massless flavours, J. High Energy Phys. 08 (2012) 096.
[211] Y. Aoki, T. Aoyama, M. Kurachi, T. Maskawa, K. i. Nagai, H. Ohki, A. Shibata, K. Yamawaki, and T. Yamazaki, Lattice study of conformality in twelve-flavor QCD, Phys. Rev. D **86**, 054506 (2012).
[212] A. Cheng, A. Hasenfratz, G. Petropoulos, and D. Schaich, Scale-dependent mass anomalous dimension from Dirac eigenmodes, J. High Energy Phys. 07 (2013) 061.
[213] T. DeGrand, Y. Shamir, and B. Svetitsky, Near the sill of the conformal window: Gauge theories with fermions in two-index representations, Phys. Rev. D **88**, 054505 (2013).
[214] A. Hasenfratz, A. Cheng, G. Petropoulos, and D. Schaich, Finite size scaling and the effect of the gauge coupling in 12 flavor systems, Proc. Sci. LATTICE2013 (**2014**) 075.
[215] T. Appelquist *et al.* (LSD Collaboration), Lattice simulations with eight flavors of domain wall fermions in SU(3) gauge theory, Phys. Rev. D **90**, 114502 (2014).
[216] M. P. Lombardo, K. Miura, T. J. Nunes da Silva, and E. Pallante, On the particle spectrum and the conformal window, J. High Energy Phys. 12 (2014) 183.
[217] A. Hasenfratz, D. Schaich, and A. Veernala, Nonperturbative β function of eight-flavor SU(3) gauge theory, J. High Energy Phys. 06 (2015) 143.
[218] A. Athenodorou, E. Bennett, G. Bergner, and B. Lucini, Infrared regime of SU(2) with one adjoint Dirac flavor, Phys. Rev. D **91**, 114508 (2015).
[219] Z. Fodor, K. Holland, J. Kuti, S. Mondal, D. Nogradi, and C. H. Wong, The running coupling of 8 flavors and 3 colors, J. High Energy Phys. 06 (2015) 019.
[220] Z. Fodor, K. Holland, J. Kuti, S. Mondal, D. Nogradi, and C. H. Wong, The running coupling of the minimal sextet composite Higgs model, J. High Energy Phys. 09 (2015) 039.
[221] J. Rantaharju, T. Rantalaiho, K. Rummukainen, and K. Tuominen, Running coupling in SU(2) gauge theory with two adjoint fermions, Phys. Rev. D **93**, 094509 (2016).
[222] J. Rantaharju, Gradient flow coupling in the SU(2) gauge theory with two adjoint fermions, Phys. Rev. D **93**, 094516 (2016).
[223] Z. Fodor, K. Holland, J. Kuti, S. Mondal, D. Nogradi, and C. H. Wong, Fate of the conformal fixed point with twelve massless fermions and SU(3) gauge group, Phys. Rev. D **94**, 091501 (2016).
[224] R. Arthur, V. Drach, M. Hansen, A. Hietanen, C. Pica, and F. Sannino, SU(2) gauge theory with two fundamental flavors: A minimal template for model building, Phys. Rev. D **94**, 094507 (2016).
[225] A. Athenodorou, E. Bennett, G. Bergner, D. Elander, C. J. D. Lin, B. Lucini, and M. Piai, Large mass hierarchies from strongly-coupled dynamics, J. High Energy Phys. 06 (2016) 114.
[226] R. Arthur, V. Drach, A. Hietanen, C. Pica, and F. Sannino, $SU(2)$ gauge theory with two fundamental flavours: Scalar and pseudoscalar spectrum, arXiv:1607.06654.
[227] A. Hasenfratz and D. Schaich, Nonperturbative β function of twelve-flavor SU(3) gauge theory, J. High Energy Phys. 02 (2018) 132.
[228] V. Leino, J. Rantaharju, T. Rantalaiho, K. Rummukainen, J. M. Suorsa, and K. Tuominen, The gradient flow running coupling in SU(2) gauge theory with $N_f = 8$ fundamental flavors, Phys. Rev. D **95**, 114516 (2017).
[229] V. Leino, K. Rummukainen, J. M. Suorsa, K. Tuominen, and S. Tähtinen, Infrared fixed point of SU(2) gauge theory with six flavors, Phys. Rev. D **97**, 114501 (2018).
[230] A. Amato, V. Leino, K. Rummukainen, K. Tuominen, and S. Tähtinen, From chiral symmetry breaking to conformality in SU(2) gauge theory, arXiv:1806.07154.
[231] Z. Fodor, K. Holland, J. Kuti, D. Nogradi, and C. H. Wong, Fate of a recent conformal fixed point and β-function in the SU(3) BSM gauge theory with ten massless flavors, Proc. Sci. LATTICE2018 (**2018**) 199.
[232] A. Hasenfratz, C. Rebbi, and O. Witzel, Gradient flow step-scaling function for SU(3) with twelve flavors, Phys. Rev. D **100**, 114508 (2019).
[233] A. Hasenfratz, C. Rebbi, and O. Witzel, Gradient flow step-scaling function for SU(3) with ten fundamental flavors, Phys. Rev. D **101**, 114508 (2020).
[234] T. Appelquist *et al.* (Lattice Strong Dynamics Collaboration), Near-conformal dynamics in a chirally broken system, Phys. Rev. D **103**, 014504 (2021).
[235] C. Lopez, G. Bergner, I. Montvay, and S. Piemonte, Measurement of the mass anomalous dimension of near-conformal adjoint QCD with the gradient flow, arXiv:2011.02815.
[236] A. Athenodorou, E. Bennett, G. Bergner, and B. Lucini, Investigating the conformal behavior of SU(2) with one adjoint Dirac flavor, Phys. Rev. D **104**, 7 (2021).
[237] E. Bennett, A. Athenodorou, G. Bergner, and B. Lucini, New lattice results for SU(2) gauge theory with one adjoint Dirac flavor, Proc. Sci. LATTICE2021 (**2022**) 204.
[238] G. Bergner, J. C. Lopez, S. Piemonte, and I. S. Calero, Lattice simulations of adjoint QCD with one Dirac overlap fermion, Phys. Rev. D **106**, 094507 (2022).

[239] E. Bennett, A. Athenodorou, G. Bergner, P. Butti, and B. Lucini, Update on SU(2) with one adjoint Dirac flavor, Proc. Sci. LATTICE2022 (**2023**) 204.

[240] G. Bergner, S. Piemonte, I. Soler Calero, and J. C. Lopez, One flavour adjoint QCD with overlap fermions, Proc. Sci. LATTICE2022 (**2023**) 206.

[241] A. Hasenfratz, E. T. Neil, Y. Shamir, B. Svetitsky, and O. Witzel, Infrared fixed point of the SU(3) gauge theory with $N_f = 10$ flavors, Phys. Rev. D **108**, L071503 (2023).

[242] Y. Aoki *et al.* (LatKMI Collaboration), Light composite scalar in eight-flavor QCD on the lattice, Phys. Rev. D **89**, 111502 (2014).

[243] T. Appelquist, R. C. Brower, G. T. Fleming, A. Hasenfratz, X. Y. Jin, J. Kiskis, E. T. Neil, J. C. Osborn, C. Rebbi, E. Rinaldi *et al.*, Strongly interacting dynamics and the search for new physics at the LHC, Phys. Rev. D **93**, 114514 (2016).

[244] Y. Aoki *et al.* (LatKMI Collaboration), Light flavor-singlet scalars and walking signals in $N_f = 8$ QCD on the lattice, Phys. Rev. D **96**, 014508 (2017).

[245] A. D. Gasbarro and G. T. Fleming, Examining the low energy dynamics of walking gauge theory, Proc. Sci. LATTICE2016 (**2017**) 242.

[246] T. Appelquist *et al.* (Lattice Strong Dynamics Collaboration), Nonperturbative investigations of SU(3) gauge theory with eight dynamical flavors, Phys. Rev. D **99**, 014509 (2019).

[247] T. Appelquist *et al.* (Lattice Strong Dynamics (LSD) Collaboration), Goldstone boson scattering with a light composite scalar, Phys. Rev. D **105**, 034505 (2022).

[248] A. Hasenfratz, Emergent strongly coupled ultraviolet fixed point in four dimensions with eight Kähler-Dirac fermions, Phys. Rev. D **106**, 014513 (2022).

[249] T. Appelquist *et al.* (LSD Collaboration), Hidden conformal symmetry from the lattice, arXiv:2305.03665.

[250] R. C. Brower *et al.* (Lattice Strong Dynamics Collaboration), Light scalar meson and decay constant in SU(3) gauge theory with eight dynamical flavors, arXiv:2306.06095.

[251] Z. Fodor, K. Holland, J. Kuti, D. Nogradi, C. Schroeder, and C. H. Wong, Can the nearly conformal sextet gauge model hide the Higgs impostor?, Phys. Lett. B **718**, 657 (2012).

[252] Z. Fodor, K. Holland, J. Kuti, S. Mondal, D. Nogradi, and C. H. Wong, Toward the minimal realization of a light composite Higgs, Proc. Sci. LATTICE2014 (**2015**) 244.

[253] Z. Fodor, K. Holland, J. Kuti, S. Mondal, D. Nogradi, and C. H. Wong, Status of a minimal composite Higgs theory, Proc. Sci. LATTICE2015 (**2016**) 219.

[254] Z. Fodor, K. Holland, J. Kuti, D. Nogradi, and C. H. Wong, The twelve-flavor β-function and dilaton tests of the sextet scalar, EPJ Web Conf. **175**, 08015 (2018).

[255] Z. Fodor, K. Holland, J. Kuti, and C. H. Wong, Tantalizing dilaton tests from a near-conformal EFT, Proc. Sci. LATTICE2018 (**2019**) 196.

[256] Z. Fodor, K. Holland, J. Kuti, and C. H. Wong, Dilaton EFT from p-regime to RMT in the ϵ-regime, Proc. Sci., LATTICE2019 (**2020**) 246.

[257] C. N. Leung, S. T. Love, and W. A. Bardeen, Spontaneous symmetry breaking in scale invariant quantum electrodynamics, Nucl. Phys. **B273**, 649 (1986).

[258] W. A. Bardeen, C. N. Leung, and S. T. Love, The dilaton and chiral symmetry breaking, Phys. Rev. Lett. **56**, 1230 (1986).

[259] K. Yamawaki, M. Bando, and K. i. Matumoto, Scale invariant technicolor model and a technidilaton, Phys. Rev. Lett. **56**, 1335 (1986).

[260] A. A. Migdal and M. A. Shifman, Dilaton effective Lagrangian in gluodynamics, Phys. Lett. **114B**, 445 (1982).

[261] S. Coleman, *Aspects of Symmetry: Selected Erice Lectures* (Cambridge University Press, Cambridge, England, 1985), ISBN: 978-0-521-31827-3.

[262] W. D. Goldberger, B. Grinstein, and W. Skiba, Distinguishing the Higgs boson from the dilaton at the Large Hadron Collider, Phys. Rev. Lett. **100**, 111802 (2008).

[263] D. K. Hong, S. D. H. Hsu, and F. Sannino, Composite Higgs from higher representations, Phys. Lett. B **597**, 89 (2004).

[264] D. D. Dietrich, F. Sannino, and K. Tuominen, Light composite Higgs from higher representations versus electroweak precision measurements: Predictions for CERN LHC, Phys. Rev. D **72**, 055001 (2005).

[265] M. Hashimoto and K. Yamawaki, Techni-dilaton at conformal edge, Phys. Rev. D **83**, 015008 (2011).

[266] T. Appelquist and Y. Bai, A light dilaton in walking gauge theories, Phys. Rev. D **82**, 071701 (2010).

[267] L. Vecchi, Phenomenology of a light scalar: The dilaton, Phys. Rev. D **82**, 076009 (2010).

[268] Z. Chacko and R. K. Mishra, Effective theory of a light dilaton, Phys. Rev. D **87**, 115006 (2013).

[269] B. Bellazzini, C. Csaki, J. Hubisz, J. Serra, and J. Terning, A Higgslike dilaton, Eur. Phys. J. C **73**, 2333 (2013).

[270] B. Bellazzini, C. Csaki, J. Hubisz, J. Serra, and J. Terning, A naturally light dilaton and a small cosmological constant, Eur. Phys. J. C **74**, 2790 (2014).

[271] T. Abe, R. Kitano, Y. Konishi, K. y. Oda, J. Sato, and S. Sugiyama, Minimal dilaton model, Phys. Rev. D **86**, 115016 (2012).

[272] E. Eichten, K. Lane, and A. Martin, A Higgs impostor in low-scale technicolor, arXiv:1210.5462.

[273] P. Hernandez-Leon and L. Merlo, Distinguishing a Higgs-like dilaton scenario with a complete bosonic effective field theory basis, Phys. Rev. D **96**, 075008 (2017).

[274] J. Cruz Rojas, D. K. Hong, S. H. Im, and M. Järvinen, Holographic light dilaton at the conformal edge, J. High Energy Phys. 05 (2023) 204.

[275] S. Matsuzaki and K. Yamawaki, Dilaton chiral perturbation theory: Determining the mass and decay constant of the technidilaton on the lattice, Phys. Rev. Lett. **113**, 082002 (2014).

[276] M. Golterman and Y. Shamir, Low-energy effective action for pions and a dilatonic meson, Phys. Rev. D **95**, 054502 (2016).

[277] A. Kasai, K. i. Okumura, and H. Suzuki, A dilaton-pion mass relation, arXiv:1609.02264.

[278] M. Hansen, K. Langaeble, and F. Sannino, Extending chiral perturbation theory with an isosinglet scalar, Phys. Rev. D **95**, 036005 (2017).

[279] M. Golterman and Y. Shamir, Effective pion mass term and the trace anomaly, Phys. Rev. D **95**, 016003 (2017).

[280] T. Appelquist, J. Ingoldby, and M. Piai, Dilaton EFT framework for lattice data, J. High Energy Phys. 07 (2017) 035.

[281] T. Appelquist, J. Ingoldby, and M. Piai, Analysis of a dilaton EFT for lattice data, J. High Energy Phys. 03 (2018) 039.
[282] M. Golterman and Y. Shamir, Large-mass regime of the dilaton-pion low-energy effective theory, Phys. Rev. D **98**, 056025 (2018).
[283] O. Cata and C. Muller, Chiral effective theories with a light scalar at one loop, Nucl. Phys. **B952**, 114938 (2020).
[284] O. Catà, R. J. Crewther, and L. C. Tunstall, Crawling technicolor, Phys. Rev. D **100**, 095007 (2019).
[285] T. Appelquist, J. Ingoldby, and M. Piai, Dilaton potential and lattice data, Phys. Rev. D **101**, 075025 (2020).
[286] M. Golterman, E. T. Neil, and Y. Shamir, Application of dilaton chiral perturbation theory to $N_f = 8$, SU(3) spectral data, Phys. Rev. D **102**, 034515 (2020).
[287] M. Golterman and Y. Shamir, Explorations beyond dilaton chiral perturbation theory in the eight-flavor SU(3) gauge theory, Phys. Rev. D **102**, 114507 (2020).
[288] T. Appelquist, J. Ingoldby, and M. Piai, Nearly conformal composite Higgs model, Phys. Rev. Lett. **126**, 191804 (2021).
[289] T. Appelquist, J. Ingoldby, and M. Piai, Composite two-Higgs doublet model from dilaton effective field theory, Nucl. Phys. **B983**, 115930 (2022).
[290] T. Appelquist, J. Ingoldby, and M. Piai, Dilaton effective field theory, Universe **9**, 10 (2023).
[291] Grid Contributors, Grid commit, 10.5281/zenodo.8136357.
[292] P. Boyle, A. Yamaguchi, G. Cossu, and A. Portelli, Grid: A next generation data parallel C++ QCD library, arXiv:1512.03487.
[293] P. A. Boyle, G. Cossu, A. Yamaguchi, and A. Portelli, Grid: A next generation data parallel C++ QCD library, Proc. Sci. LATTICE2015 (**2016**) 023.
[294] A. Yamaguchi, P. Boyle, G. Cossu, G. Filaci, C. Lehner, and A. Portelli, Grid: OneCode and FourAPIs, Proc. Sci. LATTICE2021 (**2022**) 035.
[295] Github Grid repository—https://github.com/paboyle/Grid (accessed 2023-06-15).
[296] R. Lewis, C. Pica, and F. Sannino, Light asymmetric dark matter on the Lattice: SU(2) technicolor with two fundamental flavors, Phys. Rev. D **85**, 014504 (2012).
[297] S. R. Coleman, J. Wess, and B. Zumino, Structure of phenomenological Lagrangians. 1., Phys. Rev. **177**, 2239 (1969).
[298] S. Weinberg, Phenomenological Lagrangians, Physica (Amsterdam) **96A**, 327 (1979).
[299] J. Gasser and H. Leutwyler, Chiral perturbation theory: Expansions in the mass of the strange quark, Nucl. Phys. **B250**, 465 (1985).
[300] H. Leutwyler, On the foundations of chiral perturbation theory, Ann. Phys. (N.Y.) **235**, 165 (1994).
[301] M. A. Luty, Strong conformal dynamics at the LHC and on the lattice, J. High Energy Phys. 04 (2009) 050.
[302] T. DeGrand, Finite-size scaling tests for SU(3) lattice gauge theory with color sextet fermions, Phys. Rev. D **80**, 114507 (2009).
[303] L. Del Debbio, B. Lucini, A. Patella, C. Pica, and A. Rago, Mesonic spectroscopy of minimal walking technicolor, Phys. Rev. D **82**, 014509 (2010).
[304] L. Del Debbio and R. Zwicky, Hyperscaling relations in mass-deformed conformal gauge theories, Phys. Rev. D **82**, 014502 (2010).
[305] L. Del Debbio and R. Zwicky, Scaling relations for the entire spectrum in mass-deformed conformal gauge theories, Phys. Lett. B **700**, 217 (2011).
[306] A. Patella, A precise determination of the psibar-psi anomalous dimension in conformal gauge theories, Phys. Rev. D **86**, 025006 (2012).
[307] A. Hasenfratz, E. T. Neil, Y. Shamir, B. Svetitsky, and O. Witzel, Infrared fixed point and anomalous dimensions in a composite Higgs model, Phys. Rev. D **107**, 114504 (2023).
[308] R. J. Crewther, Genuine dilatons in gauge theories, Universe **6**, 96 (2020).
[309] L. Del Debbio and R. Zwicky, Dilaton and massive hadrons in a conformal phase, J. High Energy Phys. 08 (2022) 007.
[310] R. Zwicky, QCD with an infrared fixed point—pion sector, arXiv:2306.06752.
[311] T. van Ritbergen, J. A. M. Vermaseren, and S. A. Larin, The four loop beta function in quantum chromodynamics, Phys. Lett. B **400**, 379 (1997).
[312] G. Mack, All unitary ray representations of the conformal group SU(2,2) with positive energy, Commun. Math. Phys. **55**, 1 (1977).
[313] T. A. Ryttov and R. Shrock, Infrared evolution and phase structure of a gauge theory containing different fermion representations, Phys. Rev. D **81**, 116003 (2010); **82**, 059903(E) (2010).
[314] J. A. M. Vermaseren, S. A. Larin, and T. van Ritbergen, The four loop quark mass anomalous dimension and the invariant quark mass, Phys. Lett. B **405**, 327 (1997).
[315] K. G. Chetyrkin and M. F. Zoller, Leading QCD-induced four-loop contributions to the β-function of the Higgs self-coupling in the SM and vacuum stability, J. High Energy Phys. 06 (2016) 175.
[316] G. Cossu, L. Del Debbio, M. Panero, and D. Preti, Strong dynamics with matter in multiple representations: SU(4) gauge theory with fundamental and sextet fermions, Eur. Phys. J. C **79**, 638 (2019).
[317] L. Del Debbio, A. Lupo, M. Panero, and N. Tantalo, Multi-representation dynamics of SU(4) composite Higgs models: chiral limit and spectral reconstructions, Eur. Phys. J. C **83**, 220 (2023).
[318] N. Cabibbo and E. Marinari, A new method for updating SU(N) matrices in computer simulations of gauge theories, Phys. Lett. **119B**, 387 (1982).
[319] T. Takaishi and P. de Forcrand, Testing and tuning new symplectic integrators for hybrid Monte Carlo algorithm in lattice QCD, Phys. Rev. E **73**, 036706 (2006).
[320] T. A. DeGrand and P. Rossi, Conditioning techniques for dynamical fermions, Comput. Phys. Commun. **60**, 211 (1990).
[321] M. Creutz, Global Monte Carlo algorithms for many-fermion systems, Phys. Rev. D **38**, 1228 (1988).
[322] N. Madras and A. D. Sokal, The Pivot algorithm: A highly efficient Monte Carlo method for selfavoiding walk, J. Stat. Phys. **50**, 109 (1988).
[323] T. Takaishi, Choice of integrator in the hybrid Monte Carlo algorithm, Comput. Phys. Commun. **133**, 6 (2000).

[324] S. Gupta, A. Irback, F. Karsch, and B. Petersson, The acceptance probability in the hybrid Monte Carlo method, Phys. Lett. B **242**, 437 (1990).
[325] B. Joo, Brian Pendleton, A. D. Kennedy, Alan C. Irving, J. C. Sexton, S. M. Pickles, and S. P. Booth (UKQCD Collaboration), Instability in the molecular dynamics step of hybrid Monte Carlo in dynamical Fermion lattice QCD simulations, Phys. Rev. D **62**, 114501 (2000).
[326] M. A. Clark and A. D. Kennedy, The RHMC algorithm for two flavors of dynamical staggered fermions, Nucl. Phys. B, Proc. Suppl. **129–130**, 850 (2004).
[327] S. Borsanyi, K. R., Z. Fodor, D. A. Godzieba, P. Parotto, and D. Sexty, Precision study of the continuum SU(3) Yang-Mills theory: How to use parallel tempering to improve on supercritical slowing down for first order phase transitions, Phys. Rev. D **105**, 074513 (2022).
[328] B. Lucini, D. Mason, M. Piai, E. Rinaldi, and D. Vadacchino, First-order phase transitions in Yang-Mills theories and the density of state method, Phys. Rev. D **108**, 074517 (2023).
[329] J. J. M. Verbaarschot, The spectrum of the QCD Dirac operator and chiral random matrix theory: The threefold way, Phys. Rev. Lett. **72**, 2531 (1994).
[330] J. J. M. Verbaarschot and T. Wettig, Random matrix theory and chiral symmetry in QCD, Annu. Rev. Nucl. Part. Sci. **50**, 343 (2000).
[331] T. Banks and A. Casher, Chiral symmetry breaking in confining theories, Nucl. Phys. **B169**, 103 (1980).
[332] M. Lüscher, Properties and uses of the Wilson flow in lattice QCD, J. High Energy Phys. 08 (2010) 071; 03 (2014) 92.
[333] .M. Lüscher, Future applications of the Yang-Mills gradient flow in lattice QCD, Proc. Sci. LATTICE2013 (**2014**) 016.
[334] B. Sheikholeslami and R. Wohlert, Improved continuum limit lattice action for QCD with Wilson fermions, Nucl. Phys. **B259**, 572 (1985).
[335] M. Hasenbusch and K. Jansen, Speeding up lattice QCD simulations with clover improved Wilson fermions, Nucl. Phys. **B659**, 299 (2003).
[336] Z. Fodor, K. Holland, J. Kuti, D. Nogradi, and C. H. Wong, The Yang-Mills gradient flow in finite volume, J. High Energy Phys. 11 (2012) 007.
[337] M. Dalla Brida *et al.* (ALPHA Collaboration), Slow running of the gradient flow coupling from 200 MeV to 4 GeV in $N_f = 3$ QCD, Phys. Rev. D **95**, 014507 (2017).
[338] A. Hasenfratz, C. Rebbi, and O. Witzel, Gradient flow step-scaling function for SU(3) with Nf = 8 fundamental flavors, Phys. Rev. D **107**, 114508 (2023).
[339] L. Del Debbio and A. Ramos, Lattice determinations of the strong coupling, Phys. Rep. **920**, 1 (2021).
[340] P. Fritzsch and A. Ramos, The gradient flow coupling in the Schrödinger functional, J. High Energy Phys. 10 (2013) 008.
[341] M. Dalla Brida, Past, present, and future of precision determinations of the QCD parameters from lattice QCD, Eur. Phys. J. A **57**, 66 (2021).
[342] M. Hansen, A. Lupo, and N. Tantalo, Extraction of spectral densities from lattice correlators, Phys. Rev. D **99**, 094508 (2019).
[343] M. T. Hansen, H. B. Meyer, and D. Robaina, From deep inelastic scattering to heavy-flavor semileptonic decays: Total rates into multihadron final states from lattice QCD, Phys. Rev. D **96**, 094513 (2017).
[344] J. Bulava and M. T. Hansen, Scattering amplitudes from finite-volume spectral functions, Phys. Rev. D **100**, 034521 (2019).
[345] G. Bailas, S. Hashimoto, and T. Ishikawa, Reconstruction of smeared spectral function from Euclidean correlation functions, Prog. Theor. Exp. Phys. **2020**, 043B07 (2020).
[346] P. Gambino and S. Hashimoto, Inclusive semileptonic decays from lattice QCD, Phys. Rev. Lett. **125**, 032001 (2020).
[347] M. Bruno and M. T. Hansen, Variations on the Maiani-Testa approach and the inverse problem, J. High Energy Phys. 06 (2021) 043.
[348] A. Lupo, M. Panero, N. Tantalo, and L. Del Debbio, Spectral reconstruction in SU(4) gauge theory with fermions in multiple representations, Proc. Sci. LATTICE2021 (**2022**) 092.
[349] P. Gambino, S. Hashimoto, S. Mächler, M. Panero, F. Sanfilippo, S. Simula, A. Smecca, and N. Tantalo, Lattice QCD study of inclusive semileptonic decays of heavy mesons, J. High Energy Phys. 07 (2022) 083.
[350] J. Bulava, M. T. Hansen, M. W. Hansen, A. Patella, and N. Tantalo, Inclusive rates from smeared spectral densities in the two-dimensional O(3) non-linear σ-model, J. High Energy Phys. 07 (2022) 034.
[351] A. Lupo, L. Del Debbio, M. Panero, and N. Tantalo, Fits of finite-volume smeared spectral densities, Proc. Sci. LATTICE2022 (**2023**) 215.
[352] E. Bennett, P. A. Boyle, L. Del Debbio, N. Forzano, D. K. Hong, J.-W. Lee, J. Lenz, C.-J. D. Lin, B. Lucini, A. Lupo, M. Piai, and D. Vadacchino, Symplectic lattice gauge theories on Grid: Approaching the conformal window—data release, 10.5281/zenodo.8136452.
[353] E. Bennett, P. A. Boyle, L. Del Debbio, N. Forzano, D. K. Hong, J.-W. Lee, J. Lenz, C.-J. D. Lin, B. Lucini, A. Lupo, M. Piai, and D. Vadacchino, Symplectic lattice gauge theories on grid: Approaching the conformal window—analysis code, 10.5281/zenodo.8136514.